# Direct conversion of Copper Carbonate substrates into porous Metal-Organic Framework HKUST-1.

Raffaele Riccò,[a] Oliver M. Linder-Patton,[b] Kenji Sumida,[b] Mark J. Styles,[c] Kang Liang,[c†] Heinz Amenitsch,[d] Christian J. Doonan,[b] and Paolo Falcaro[a*]

a. Institute of Physical and Theoretical Chemistry, Technical University Graz, Stremayrgasse 9, 8010 Graz, Austria.

b. Centre for Advanced Nanomaterials, School of Physical Sciences, The University of Adelaide, North Terrace Campus, Adelaide SA 5005, Australia.

c. CSIRO Manufacturing, Private Bag 10, Clayton South 3169, Victoria, Australia.

d. Institute of Inorganic Chemistry, Graz University of Technology, Stremayrgasse 9, 8010 Graz, Austria.

*Supporting Information Placeholder*

**ABSTRACT:** The preparation of microporous metal-organic frameworks (MOFs) at industrial scales requires careful selection of the metal precursor to ensure the sustainability of the synthetic process, in terms of both the environmental impact and cost. The use of earth abundant minerals is attractive for this purpose, provided that they are sufficiently reactive under the conditions of MOF formation. In this work, we investigate the use of copper carbonate and its naturally-occurring counterparts, malachite and azurite, as precursors for the synthesis of $Cu_3(btc)_2$ (HKUST-1; $btc^{3-}$=1,3,5-benzenetricarboxylate). Using a water/ethanol solution of copper carbonate and $H_3btc$, HKUST-1 was obtained at room temperature within 3 hrs, as confirmed by a suite of characterization techniques. The identity of the products was determined by the reaction conditions, highlighting the importance of optimizing the synthetic parameters. When prepared under optimized conditions, HKUST-1 synthesized here showed analogous performance characteristics to materials obtained by traditional solvothermal methods, thus our results confirm that high-quality samples of MOFs can be easily derived from mineral precursors.

## INTRODUCTION

The high accessible surface areas and chemical tunability of metal-organic frameworks (MOFs)[1] has motivated researchers to explore their potential for application to gas storage,[2] molecular separations,[3] catalysis,[4] drug delivery,[5] biotechnology,[6] and device fabrication.[7] As the field of MOF chemistry matures and they approach commercial implementation,[8–10] synthetic pathways for large-scale preparation has come under great scrutiny.[11–15] Traditional laboratory-scale preparations involve the reaction of metal salts (typically a metal halide or nitrate) and an organic ligands in a polar solvent such as DMF. The waste products from such reactions include harsh acids and environmentally harmful organic compounds.[1,16] Therefore, faster, greener and more economically affordable processes that do not require expensive purification steps are attractive, especially given the increasingly stringent regulations surrounding environmental management and worker health (i.e. REACH[17] and RoHS[18] directives). These driving forces have contributed to the development of alternative synthetic techniques for MOFs, including electrochemical methods[19] flow synthesis,[14,20] the use of aqueous media,[21,22] and solvent-free mechanochemical synthesis,[23,24]

Following the direction of aqueous or solvent free reactions, MOFs obtained via the direct conversion of ceramic precursors has garnered significant interest[25] as an alternative to the traditional solvothermal approach. A crucial pioneering work in this field by Furukawa and coworkers showed how periodic alumina inverse opals can be transformed into Al-based MOF hierarchical structures. The process, named *pseudomorphic replication*, was performed in water with microwave assistance and proceeded via the dissolution of the ceramic (and liberation of metal ions from the solid-liquid interface) followed by the rapid crystallization of the MOF at the surface of the parent phase.[26] The obtained MOF inverse opal was used for water *vs.* ethanol separation. Another major breakthrough in this field was reported by Ameloot and coworkers. In this case they employed a chemical vapor approach to convert zinc oxide thin films (synthesized using Atomic Layer Deposition) into zeolitic imidazolate framework 8 (ZIF-8) by exposure of the ceramic to vapors of 2-methylimidazole; a salient feature of this solvent-free process is that it is considered to be compatible with current microelectronic fabrication technology.[27] Non-oxide inorganic phases can also be used as a precursor for MOF synthesis. For example, in collaboration with Takahashi's group, we converted a film of aligned copper hydroxide nanostructures into oriented $Cu_2(bdc)_2$ ($bdc^{2-}$ = 1,4-benzenedicarboxylate) crystals. The anisotropic properties of the aligned polycrystalline MOF film was demonstrated via the fabrication of an optical switch.[28]

These three examples show how different ceramic precursors can influence the structure and, as a result, impart unique functional properties, to the resulting MOF material.[25]

Among the different feedstock ceramic materials, metal carbonates are found as minerals (e.g. dolomite, calcite, aragonite, magnesite), and relevant ores in industry (e.g. siderite, smithsonite, rhodochrosite). Additionally, the conversion of carbonates into MOFs is attractive as the primary by-products are water and carbon dioxide. Nevertheless, the use of carbonates to synthesize MOFs is largely unexplored.[29] The first carbonate conversion into MOF was performed by Sumida *et al.*, who uncovered the process by which $CaCO_3$ can undergo coordination replication, to terephthalate or squarate based MOFs,[29] using microwave heating with temperatures starting from 100 °C. To make this process more versatile conversion at room temperature is desirable as it would be less energy consuming and allow for the preparation of MOF composites from temperature-sensitive species (e.g. biomacromolecules)[30] or substrates (paper, plastic).[31]

Copper carbonate minerals such as malachite ($Cu_2CO_3(OH)_2$)[32] and azurite ($Cu_3(CO_3)_2(OH)_2$)[33] are widespread and commonly found within copper ores. Due to their abundance and bright green and blue colors, respectively, they have been used as pigments since antiquity.[34] Moreover, malachite is commercially available as the finely powdered green basic copper carbonate.

**Scheme 1. Representation of the conversion from basic copper carbonate (left) to HKUST-1 MOF (right) upon reaction with trimesic acid (1,3,5-benzenetricarboxylic acid, center) in a solvent mixture of water and ethanol.**

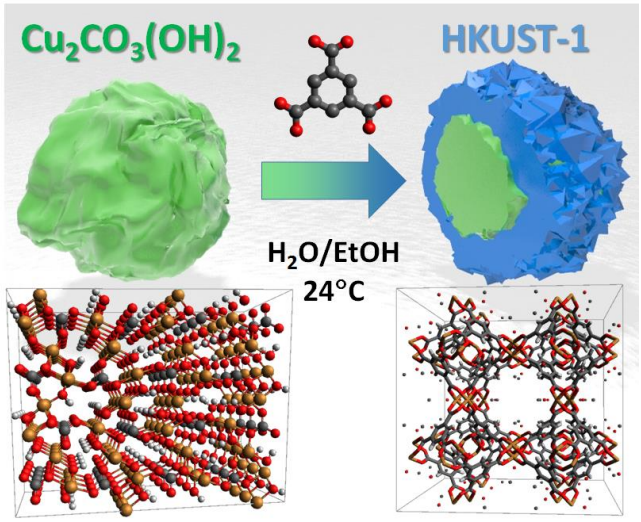


An additional motivation to focus on Cu-based MOFs is that literature precedent has shown that copper-based substrates can be promptly converted into HKUST-1. For example, copper metal substrates were at first converted to hydroxides using a basic oxidizing solution, then directly converted into HKUST-1 by immersion into an alcohol/water mixture with trimesic acid.[35] Additionally, copper hydroxide based monoliths were directly replicated into HKUST-1 by immersion in an organic solution of trimesic acid.[36] Another study showed that patterns of insoluble copper nitrate hydrate powders could be converted into MOF powders.[37] Finally, a continuous crack-free membranes could be fabricated by converting CuO nanosheets into HKUST-1 using a solution of trimesic acid in ethanol and water, and sodium formate as an additive. [38]

Here we show the straightforward conversion of basic copper carbonate into HKUST-1 (**Scheme 1**). The process involves addition of synthetic basic copper carbonate (BCC) powder to a solution of benzene-1,3,5-tricarboxylic acid ($H_3btc$) prepared in a water/ethanol mixture. By adjusting the amount of BCC powder, solvent ratio, reaction temperature and time, the morphology and surface area of the resulting HKUST-1 products can be controlled. Furthermore, the integrity of the carbonate–derived HKUST-1 was confirmed by comparing its Lewis acid catalytic performance to HKUST-1 prepared by standard solvothermal synthesis.[39]. Lastly, we also show that this synthetic strategy can be successfully extended to natural copper based carbonate minerals such as malachite and azurite.

## Experimental Details

**Materials and methods.** Basic copper carbonate monohydrate (BCC, $Cu_2CO_3(OH)_2{\cdot}H_2O$), benzene-1,3,5-tricarboxylic acid ($H_3btc$), 2-aminobenzophenone (2-ABP), acetylacetone (Acac), ethyl acetate, dichloromethane, n-hexane and ethanol were purchased from Sigma Aldrich and used as received. Deionized water (18 MΩ) was produced from a Millipore Synergy purification system. Malachite ($Cu_2CO_3(OH)_2$) was obtained from Cloud River Minerals (Canberra, ACT, Australia). Azurite ($Cu_3(CO_3)_2(OH)_2$) was obtained from Unique Gems and Minerals (Granville, NSW, Australia).

Unless specified, in the following synthetic protocols, the reactants were combined at room temperature (24 °C) and reacted for 3 h with gentle stirring at 20 rpm using a tube rotator (Labnet Inc.® Revolver). The resulting materials were then washed twice with EtOH and dried at 90 °C for 2 hours in an oven.

**Synthesis of HKUST-1, $Cu_3(btc)_2$, from basic copper carbonate.** In a typical procedure, 200 mg (0.84 mmol) of BCC was dispersed in a solution of 210 mg (1.00 mmol) of $H_3btc$ in 6.5 mL of a EtOH/water 1:1 solvent mixture. Variations in the carbonate amount (10, 20, 50, 100, 200, 500, 1000, and 2000 mg), temperature (-78, 0, 24, 40, 60, and 80 °C), solvent composition (EtOH/water 0:100, 25:75, 50:50, 75:25, and 100:0), and time (20 minutes, 1, 3, 6, and 24 hours) were applied to the typical procedure to ascertain the effect of the reaction conditions on the resulting products.

**Conversion of malachite and azurite minerals into HKUST-1.** Malachite (452.6 mg) or azurite (94.7 mg) minerals were finely ground and passed through a 40 mesh sieve, then dispersed in a solution of $H_3btc$ in EtOH/water 1:1 (2.1 g in 65 mL of solvent mixture). 3.08 mL and 14.7 mL of this solution were used respectively for malachite or azurite.

**Catalytic testing of HKUST-1 samples.** Samples were purified and activated according to the following procedure. The reaction mixture was centrifuged for 1 min at 1000 rcf, then EtOH was added (2.5 mL for every 100 mg of solid product) and the solid was shaken for 10-20 s using a vortex mixer at 3000 rpm (VELP Scientifica® RX3). After a further centrifugation step, the EtOH treatment was repeated twice and the wet solid was immersed in about 3 mL of dichloromethane for 24 h. This washing procedure was repeated twice with fresh solvent. After discarding the solvent, the wet solid was dried in the air, and then placed in an oven at 100 °C overnight (15 hours).

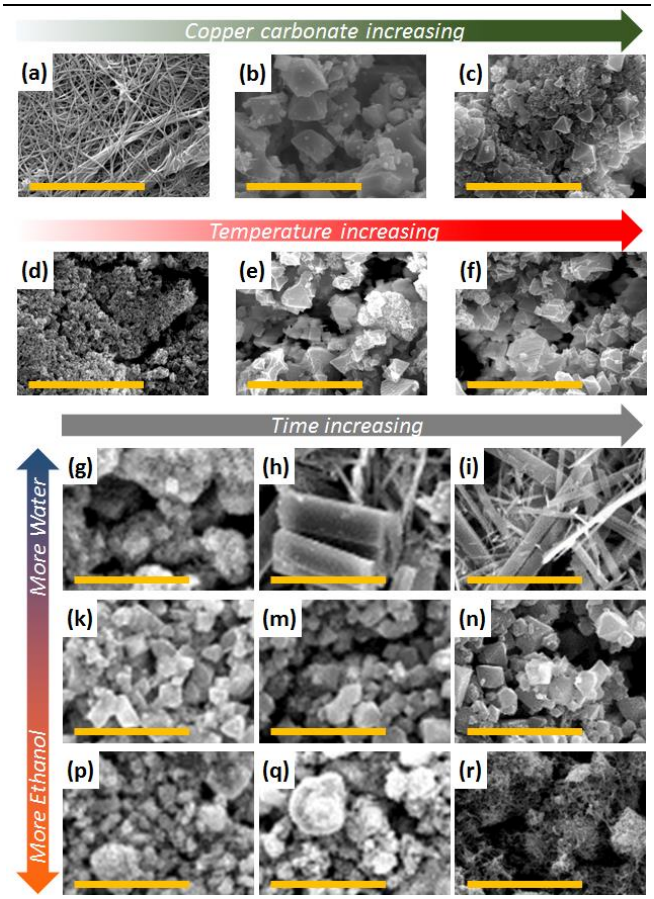


**Figure 1.** SEM micrographs of HKUST-1 MOF ($Cu_3btc_2$) obtained from basic copper carbonate by conversion using 6.5 mL of H3btc solution with (a-c) different amounts of copper carbonate (a: 20 mg, b: 200 mg, c: 2000 mg), (d-f) different temperatures (a: -78 °C, b: 24 °C, c: 80 °C), and different amount of EtOH (g,h,i: 0% EtOH; k,m,n: 50% EtOH; p,q,r: 100% EtOH), with different reaction times (g,k,p: 20 minutes; h,m,q: 3 hours; i,n,r: 24 hours). For pictures a-f, the reaction time was three hours. Scalebar: 10 µm (see Supplementary Information Figure S2-S4 for a complete survey).

**Friedländer reaction with HKUST-1 as catalyst.** The reaction was performed according to literature methods.[40] In a typical procedure, 50.0 mg (0.0827 mmol, equivalent to 0.248 mmol Cu(II)) of activated HKUST-1 were mixed with 500 mg (4.99 mmol) of Acac. Under stirring, 197 mg (1.00 mmol) of 2ABP was added and the reaction mixture heated at 80 °C for three hours (TLC: EtOAc/n-hexane 1:2 as eluent, $R_f$ = 0.5). After cooling, EtOH (1 mL) was added and the reaction mixture centrifuged (4000 rcf, 10 min) to remove the catalyst, then the solvent was removed under vacuum. The solid residual was dissolved in dichloromethane, (DCM - 5 mL) and filtered twice over cotton, then dried under vacuum overnight. The conversion was calculated,[35] by dissolving the resulting product mixtures in deuterated chloroform, CDCl3, and analyzing the by $^1$H-NMR spectrum of the mixture (using a Bruker Avance III 300 MHz NMR spectrometer). The most suitable integrals used to evaluate the catalytic activity were calculated from the signals at ≈6.7 ppm (proton in position 3 for the 2-aminobenzophenone reactant) and ≈8.4 ppm (proton in position 8 for the 2-methyl-3-acetyl-4-phenylquinoline product).

**Scanning Electron Microscopy (SEM).** Sample morphology was assessed using a field emission scanning electron microscope (FE-SEM; Merlin; Carl Zeiss Germany). Prior to SEM investigation, samples were sputter coated with iridium.

**Powder diffraction (XRD) analysis.** High-resolution X-ray powder diffraction measurements were performed at the Australian Synchrotron.[41] Samples were packed into 0.3 mm diameter capillaries and studied in Debye–Scherrer geometry. A highly monochromatic beam with a wavelength λ = 0.736826 Å was used, and data were collected using the Mythen curved position sensitive detector[42] over the range 1.5 to 81.5° 2θ (Q = 2.2 to 111.3 $nm^{-1}$). Diffraction patterns were collected for 120 s each, and were analyzed using the Rietveld method,[43] as implemented in the Topas software package (Bruker).

**Small- and Wide- Angle X-Ray Scattering (SAXS/WAXS) analysis.** Small- and wide- angle X-ray scattering (SAXS/WAXS) measurements were performed at the Austrian SAXS beamline of the electron storage ring Elettra (Trieste, Italy)[44] using 8 keV branch corresponding to a wavelength of 1.54 Å; 1 s exposure time was used to collect the diffraction image. Data were analyzed using Igor Pro software Package (WaveMetrics Inc.).

**Fourier transform infrared (FTIR) analysis.** The measurements were performed using a Bruker ALPHA FT-IR spectrometer (Bruker Optik GmbH) in transmission mode. 128 scans were performed with 2 $cm^{-1}$ intervals.

**Surface area and pore size analysis.** The $N_2$ adsorption isotherms were measured using a Micromeritics 3-Flex analyzer (Micromeritics Instrument Corporation, Norcross, GA, USA) at 77 K. Brunauer–Emmett–Teller (BET)[45] surface areas were calculated using experimental points at a relative pressure that follows the Rouquerol criteria.[46] The pore size distribution was calculated by the Barrett–Joyner–Halenda (BJH) method.[47] Detailed data are reported in Table S1 of the Supporting Information

## Results and Discussion

**Investigation of synthetic parameters.** *Reactant amounts.* To initially evaluate the appropriate copper carbonate/trimesic acid ratio for the conversion to HKUST-1, a set of experiments were conducted using a solution prepared by dissolving 210 mg of $H_3btc$ in 6.5 mL of a 1:1 mixture (in volume) of EtOH and water. The amount of copper carbonate tested was varied as follows: 10, 20, 50, 100, 200, 500, 1000 and 2000 mg (Figure S1 and S2 of the Supplementary Information) and the reaction conditions temperature (24 °C) and Time (3 hours) were fixed. SEM images (**Figure 1a-c**) show how the morphology is dependent on the amount of carbonate (20, 200, 2000 mg) added to the ligand solution. The fiber-like structures in **Figure 1a** were obtained using 20 mg of carbonate (Cu/ligand ratio = 0.1), whereas discrete crystals in **Figure 1b** can be produced using 200 mg of carbonate (Cu/ligand ratio = 1). Further increasing the amount of carbonate, up to 2000 mg, (Cu/ligand ratio = 10) did not influence on the morphology of the HKUST-1 crystals obtained. However, the clusters of crystals shown in **Figure 1c** suggests the presence of a BCC unreacted core, furthermore, visual inspection of these powders revealed a green color that is distinct from HKUST-1. Together, this data supports the incomplete conversion from the original BCC.

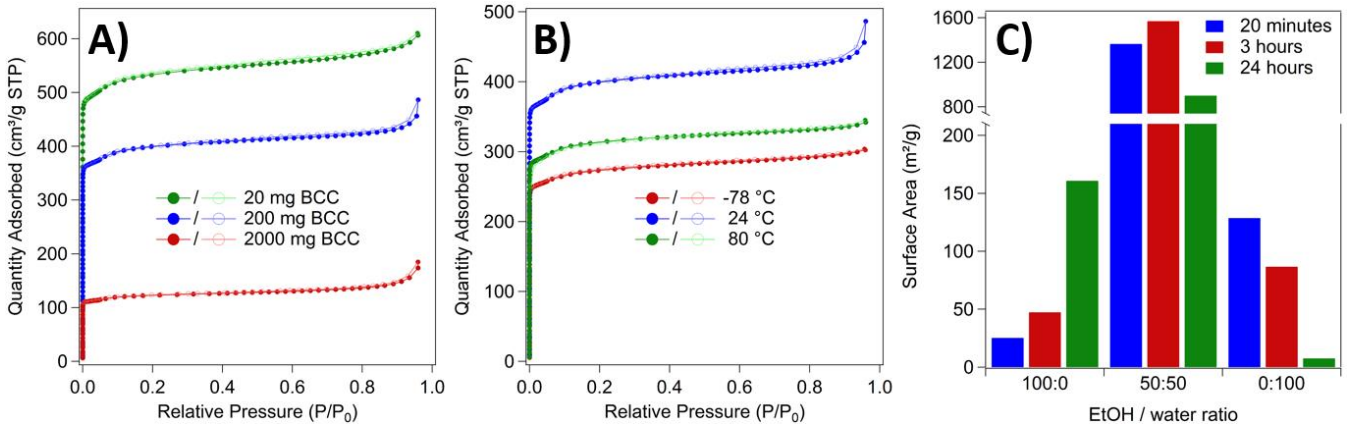


**Figure 2.** $N_2$ isotherms at 77K of the carbonate (BCC) to HKUST-1 conversion (a) with different amount of copper carbonate (a) and at different temperatures (b). The surface area for the study at different solvent ratio and times is reported in (c). Complete isotherms and additional data is provided in the Supporting Information Section (Figure S5 and Table 1).

BET surface area measurement of samples prepared from 20 mg of copper carbonate afforded an accessible surface area of 2090±5 $m^2g^{-1}$. However, further increasing the amount of carbonate to 200 and 2000 mg resulted in a decrease of the surface area to 1570±5 and 480.6±5 $m^2\ g^{-1}$, respectively. This reduction in $N_2$ uptake per g of sample can attributed to the presence of unconverted, non-porous, copper carbonate (**Figure 2a**).

*Reaction temperature.* Temperature can be employed as a parameter to control the morphology of MOF crystals.[48–50] To assess the influence of temperature on the morphology of HKUST-1, we performed conversions from copper carbonates at -78, 0, 24, 40, 60 and 80 °C (Figure S3 of the Supplementary Information shows the related SEM image) while fixing the amount of BCC to 200 mg. The morphologies obtained at -78, 24 and 80 °C are reported in **Figure 1d-f**. The material synthesized at the lowest temperature (**Figure 1d**) is indeed morphologically different from the one produced at room temperature (**Figure 1e**). On the other hand, increasing the temperature above ambient produced only a slight increase in particle size (**Figure 1f**). Room temperature (24 °C) treatment showed the largest BET surface area (1570±5 $m^2\ g^{-1}$ *vs.* 1080.0±5 $m^2\ g^{-1}$ for the -78 °C and 1230.0±5 $m^2\ g^{-1}$ for the 80 °C, **Figure 2b**). These data show that a substantial decrease or increase of the conversion temperature resulted in ca. 30% and 20% loss in the $N_2$ uptake, relative to room temperature (24 °C).

*Reaction solvent.* It is well known that the solvent plays a significant role in the growth of MOF crystals.[48,51] For example, water was found to modulate the stability of different facets in HKUST-1, thus giving rise to different morphologies.[52–54] Motivated by this knowledge, we investigated the conversion of copper carbonates under different solvent mixtures of EtOH and water. EtOH percentages were varied as follows; 0%, 25%, 50%, 75%, and 100% (**Figure 1g-r**. The complete table with the related SEM images is reported in Figure S4 of the Supplementary Information). **Figure 1g,k,p** represents the crystal morphology after 20 minutes for 0, 50, and 100% EtOH, respectively. Globular clusters are observed and increasing the amount of ethanol results in a decrease of particle size. However, it is evident that the reaction time showed a clear trend irrespective of the solvent used; the longer the reaction time the larger the crystals (**Figure 1p,q,r**). In case of pure water (**Figure 1g,h,i**), globular particles with platelet surface evolved into a rod-like morphology over time. For the 50% EtOH mixture (**Figure 1k,m,n**) the typical octahedral morphology of HKUST-1 becomes more evident after 3 hours. We examined the speed of conversion from BCC into HKUST-1 of samples produced from different solvent mixtures by 77K N2 isotherm experiments. BET surface area analysis (**Figure 2c**) revealed that MOF formation is slower when using only ethanol as a solvent (Figure S5a of the Supplementary Information). A small increase in the $N_2$ uptake is observed as the BET surface area increases from 25±5 $m^2\ g^{-1}$ after 20 min to 160±5 $m^2\ g^{-1}$ after 24 hours. However, the BET surface areas of samples synthesized in a 50:50 mixture of EtOH/water initially increases from 20 min (1365±5 $m^2\ g^{-1}$) to 3 hours (1569±1 $m^2\ g^{-1}$) and then decreases at 24 hours (900±5 $m^2\ g^{-1}$) (see Figure S5b of the Supplementary Information). When using only water as solvent (see Figure S5c of the Supplementary Information), the surface area was initially low (130±5 $m^2\ g^{-1}$ after 20 minute conversion time) and then decreased to 10±1 $m^2\ g^{-1}$ after 24 hours, becoming almost non-porous to $N_2$. This significantly reduced porosity over reaction time is expected as a result of the instability of the HKUST-1 in water.[55,56]

From these results, the optimal reaction conditions to produce small, regular, and relatively monodisperse crystal particles were found to be the following: addition of 200 mg of basic copper carbonate to a trimesic acid solution composed of a 1:1 EtOH/water mixture at room temperature for 3 hours (**Figure 1m**).

**Influence of water on HKUST-1 stability.** To assess the detrimental effect of pure water on HKUST-1, we treated a sample for 24 hours in water; the MOF was synthesized from 200 mg of copper carbonate in 6.5 mL of 50:50 EtOH/water mixture containing the $H_3BTC$ ligand at 24 °C for 3 hours The BET surface area significantly dropped from 130±5 $m^2\ g^{-1}$ to 65±5 $m^2\ g^{-1}$ (see Figure S6a of the Supplementary Information), showing a dramatic 95% reduction and supporting the previous observations reported in **Figure 2c**. Additionally, we examined the XRD patterns of HKUST-1 before and after the 24 hour washing treatment (see Figure S6b of the Supplementary Information). These data show a shift in the diffraction peaks (smaller unit cell) in the lower angle side of the XRD pattern, indicating that a topological change occurred.

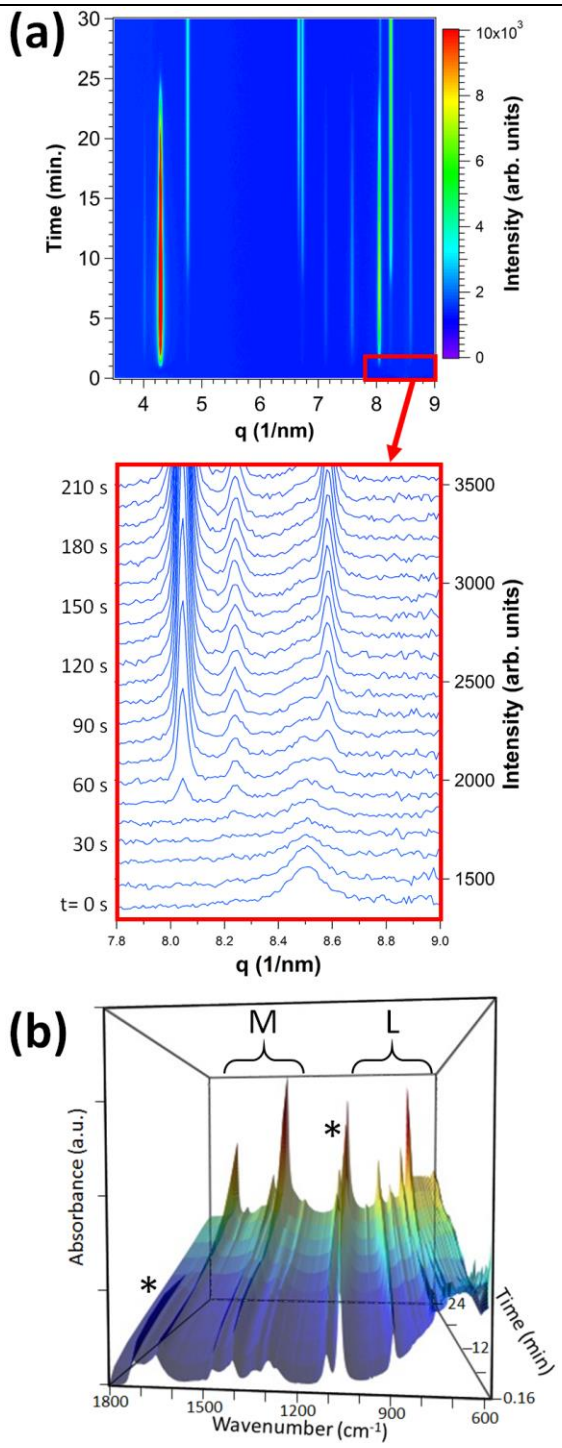


**Figure 3.** a) SAXS/WAXS kinetics in the first 30 minutes of reaction of the carbonate to HKUST-1. The magnification (red box) show the disappearance of the carbonate peak at 8.5 $nm^{-1}$ during the first minute of reaction, and the appearance of the intermediate peaks at 8.0 and 8.6 $nm^{-1}$, and the (222) HKUST-1 peak at 8.2 $nm^{-1}$; b) FTIR kinetics in the first 24 minutes of conversion, with regions attributable to the metal sites and the ligands, respectively. The bands indicated with an asterisk (*) are associated to the residual intermediate material. Detailed FTIR spectra are available in Supplementary Figure S13.

Water is essential for HKUST-1 formation, capping the copper-copper paddlewheel in the SBU of HKUST-1.[57,58] However, continued HKUST-1 formation from copper carbonate monohydrate slowly releases $H_2O$ into the reaction mixture, that has an effect on the topology and porosity of the products, as observed by the different powder patterns and the decrease in $N_2$ adsorption, when the reaction time is extended to 24 hours.

**Conversion from minerals to HKUST-1.** We also successfully converted two naturally occurring minerals, malachite and azurite into HKUST-1, using the same procedure described for commercial copper carbonate (see Figure S7 of the Supplementary Information). The resulting HKUST-1 showed reasonable $N_2$ adsorption at 77K and BET surface areas of 340±5 and 740±5 $m^2\ g^{-1}$, for malachite and azurite, respectively (see Figure S8 and Table S1 of the Supplementary Information). These values are lower than those for HKUST-1 formed from the conversion of copper carbonate. We submit that this is due to unconverted mineral or other mineral inclusions (i.e. impurities)[59] that are not reactive under the tested conditions. It is noteworthy that the substrates did not undergo any preliminary treatment, other than crushing into powder, before reaction.

**Kinetics of the Conversion Process.** In order to assess the conversion from BCC to HKUST-1, an *in situ* SAXS/WAXS analysis was conducted with a recirculation setup (dynamic conditions, see Figure S9 of the Supporting Information section). The initial carbonate precursor (large peak at c.a. 8.5 $nm^{-1}$) disappeared within 60 seconds from the injection of the H3btc ligand solution (as evidenced from the magnification box in **Figure 3a**). Surprisingly, an intermediate of reaction appeared in the first 25 minutes period of reaction, with a dominant peak at about q = 4.2 $nm^{-1}$ (maximum intensity reached at c.a. 8 min); this peak disappeared completely after ca. 28 minutes (see **Figure 3a** and Figure S10). At the same time, the evolution of HKUST-1 (monitored using the (222) peak at q = 8.2 $nm^{-1}$) was found to be slow for the first 8 minutes, after which the intensity rapidly increased to 85% of the maximum value detected within ca. 20 minutes (see Figure S11). We believe that this intermediate species was also observed by Stolar and coworkers,[60] during the synchrotron investigation of the liquid-assisted mechanosynthesis of HKUST-1. In that work after grinding $Cu(OH)_2$ with $H_3btc$ in presence of ethanol, an intermediate with a layered structure was identified. Comparing the X-ray plots, the peaks attributed to our intermediate (q = 4.3, 6.7, 8.1, and 8.6 $nm^{-1}$) are found at the same position to Stolar's intermediate; from our in-situ investigation, this phase persisted for 25 minutes before disappearing, a time that is similar to the intermediate in literature (i.e. 20 minutes).

The *in situ* XRD analysis conducted in capillary (static conditions see Figure S9 of the Supporting Information section) at the Powder Diffraction Beamline of the Australian Synchrotron showed more evidently the presence of this intermediate, which peaks disappearing similarly to the SAXS/WAXS experiments, along with the appearance of peaks attributable to HKUST-1, especially the intense peaks of the (200), (220) and (222) planes between q = 4.5 and 8.5 $nm^{-1}$ (Figure S12a). These HKUST-1 peaks increased in intensity until plateauing after 30 minutes. Rietveld refinements of the last frame of the kinetics (see Figure S12b in the Supplementary Information) confirmed that the product matches the diffraction pattern of HKUST-1.

In order to gain further insights into this growth mechanism, the reaction kinetics was also studied by FTIR experiments. Data collected in the first 24 minutes of the reaction (**Figure**

**3b** and Figure S13 of the Supporting info) showed that, along with some residual carbonate, HKUST-1 can be detected from the typical bands observed in the 1350-1750 $cm^{-1}$ region, which vibrational modes indicated the symmetric bidentate mode of coordination towards the two Cu sites,[61] and in the 650-1150 $cm^{-1}$ region with new stretching modes coming from the trimesic ligand.[37] After 10 seconds of reaction the first bands started to appear, confirming the observations taken during the XRD and SAXS/WAXS experiments of the quick onset of this conversion. The trend showing the consumption of the feedstock during the formation of the MOF is in agreement with our previous studies where we observed the production of HKUST-1 from copper hydroxide produced on Cu substrates,[35] and from copper insoluble complexes.[37] We also noted this conversion process is significantly faster than the recent process developed from CuO sheets.[38]

**Catalytic activity.** HKUST-1 is a well-known catalyst for organic reactions, due to its Lewis acidity.[62,63] The Friedländer reaction[64] has been used to test the performance of this MOF catalyst in the production of quinolines.[40] Here, HKUST-1 MOFs obtained from different sources, classic solvothermal synthesis (*sol_HKUST-1*),[39] conversion of commercial basic copper carbonate (*BCC_HKUST-1*), and conversion from malachite and azurite minerals (*mal_HKUST-1* and *azu_HKUST-1*, respectively)), were assessed, via proton NMR spectroscopy, for their capacity to catalyse the condensation between 2-aminobenzophenone (2ABP) and acetylacetone (Acac, reaction in **Figure 4**) at 80 °C, to produce 2-methyl-3-acetyl-4-phenylquinoline. The integrals of the proton in position 3 of the 2ABP (○) and in position 8 of the resulting quinoline (◊) were conveniently measured by NMR spectroscopy, thanks to the shift of its signal from ≈6.7 ppm to ≈8.1 ppm (Figure S14 of the Supplementary Information). Copper sulphate and $H_3BTC$ ligand were also evaluated, along with a reaction performed without catalyst.

The MOF obtained from solvothermal synthesis (blue bar) performed as expected, with a nearly 92% of conversion from 2ABP to the quinoline. HKUST-1 from the basic copper carbonate (teal bar) yielded for ca. 74% of conversion after 3 hours, thus representing a very good performing catalyst comparable to HKUST-1 obtained the classic way. The $Cu_3(btc)_2$ obtained from the mineral sources malachite (green bar) and azurite (cyan bar) showed a very good activity of 80% conversion, in line with the commercial carbonate and in agreement with our previous measurements performed on HKUST-1 grown on Cu metal.[35] Notably, the original carbonates (commercial or natural) did not show appreciable catalytic activity (below 7% of conversion, and comparable with the conversion obtained in absence of any catalyst), confirming Cu(II) Lewis-acid centers are essential for this reaction[62,65] (using the soluble sulfate salt the reaction was nearly quantitative) and that, more importantly, the $H_3btc$ ligand must be present to permit the substrate to interact with the copper vacancy coordination sites, through the pores.

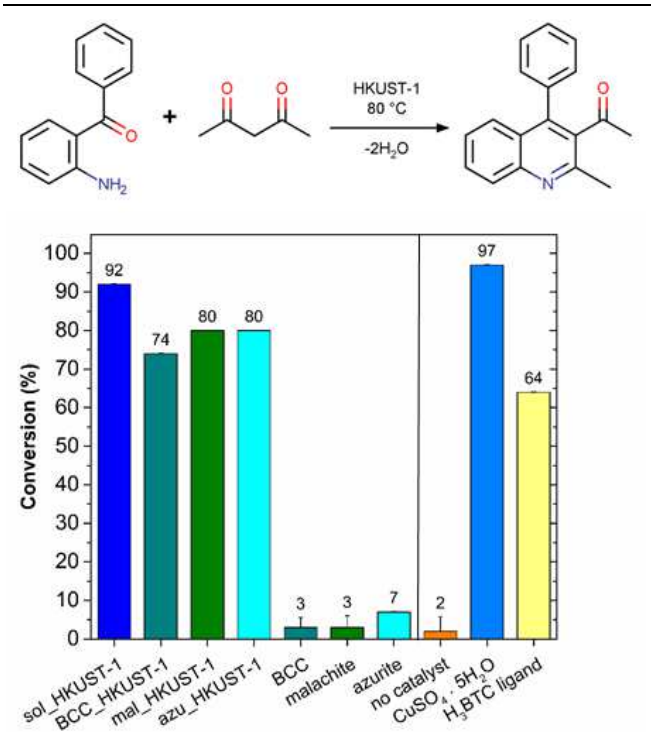


**Figure 4**. Catalytic performance in the Friedländer condensation between 2ABP and Acac (as percentage of quinoline produced from the aminophenone) of sol_HKUST-1 (blue, from solvothermal synthesis), BCC_HKUST-1 (teal, from basic copper carbonate), mal_HKUST-1 (green, from malachite), azu_HKUST-1 (cyan, from azurite), and their carbonate sources. The reaction was also performed without catalyst (orange), in presence of coppers sulfate (light blue), or the H3BTC ligand (light yellow). Reaction conditions: 2ABP/Acac/HKUST-1 molar ratio: 5:1:0.083.

This reaction can also be catalyzed by Brønsted acids, and in this case 64% conversion was obtained using the tricarboxylic acid, however, as shown in Figure 4. the Lewis-acid pathway was more efficient.

Leaching from the catalyst (either metal ions or ligands) was evaluated by collecting 100 µL of the mother liquor after the first reaction and adding them into the same reaction mixture of 2ABP and Acac. The conversions in all cases were below 7% (see Figure S15 of the Supplementary Information), with the obvious exception of the copper sulfate catalyst (24%) due to the ease of reaction of Cu(II) with Acac,[66] and the consequent increased solubility in the reaction mixture (acetylacetone also acted as solvent).

## Conclusion

Here we have described a facile process to directly convert copper carbonate into the Cu-based MOF, HKUST-1. This reaction was performed in a 1:1 mixture of ethanol and water. Although a typical 3-hour reaction was used to ensure a quantitative conversion, synchrotron XRD analysis evidenced the diffraction peaks of copper carbonate disappears within 25 minutes. The current process circumvents the use of polluting solvents and complex processes using inexpensive industrially available precursors. Parameters such as copper carbonate/ligand ratio, temperature, and solvent mixture were optimized and BET analysis on the resulting materials showed

excellent surface area results. The same reaction was successfully conducted on mineral sources of copper carbonate like malachite and azurite, showing a remarkable conversion also from these substrates. Eventually, HKUST-1 MOFs obtained from synthetic basic copper carbonate, malachite, and azurite excellently performed as Lewis acid catalysts for the Friedländer reaction up to 80% of conversion after 3 hours of reaction. Considering that the minerals underwent no preliminary purification processes, and were directly converted into MOF, the obtained results hold promise for the future exploitation of minerals as cheap and readily available sources for MOF synthesis, permitting further improvements in the catalytic activity of this copper-based framework system. In summary, this present work clearly shows that room temperature conversion is an efficient way to exploit mineral ores for the production of MOFs.

## ASSOCIATED CONTENT

### Supporting Information

SEM images of the HKUST-1 synthesis under different conditions; photographs of the HKUST-1 obtained with different carbonate amounts; photograph of azurite and malachite minerals before and after conversion; FTIR analysis; initial and final Rietveld refinements of the XRD kinetics study; additional BET data; $^1$H-NMR data of the Friedländer reaction; leaching test data. This material is available free of charge via the Internet at http://pubs.acs.org.

## AUTHOR INFORMATION


### Corresponding Author

* E-mail: paolo.falcaro@tugraz.at

### Present Address

† School of Chemical Engineering, The University of New South Wales, Sydney NSW, Australia


### Author Contributions

The manuscript was written through contributions of all authors. All authors have given approval to the final version of the manuscript.

## ACKNOWLEDGMENT


Part of this research was undertaken on the SAXS beamline of Elettra Synchrotron in Trieste, Italy, and on the Powder Diffraction and SAXS/WAXS beamlines at the Australian Synchrotron, Victoria, Australia, with support by Nigel Kirby and Justin Kimpton. Martin Thonhofer at TU Graz is acknowledged for the support in acquiring NMR data. RR acknowledges the European Union's Horizon 2020 research and innovation programme under the *Marie Skłodowska-Curie* grant agreement #748649 (project "*MNEMONIC*").


## REFERENCES


(1) Li, H.; Eddaoudi, M.; O'Keeffe, M.; Yaghi, O. M. Design and Synthesis of an Exceptionally Stable and Highly Porous Metal-Organic Framework. *Nature* **1999**, *402* (6759), 276–279.

(2) Murray, L. J.; Dincă, M.; Long, J. R. Hydrogen Storage in Metal–organic Frameworks. *Chem. Soc. Rev.* **2009**, *38* (5), 1294–1314.

(3) Li, J.-R.; Sculley, J.; Zhou, H.-C. Metal–Organic Frameworks for Separations. *Chem. Rev.* **2012**, *112* (2), 869–932.

(4) Lee, J.; Farha, O. K.; Roberts, J.; Scheidt, K. A.; Nguyen, S. T.; Hupp, J. T. Metal-Organic Framework Materials as Catalysts. *Chem. Soc. Rev.* **2009**, *38* (5), 1450–9.

(5) Della Rocca, J.; Liu, D.; Lin, W. Nanoscale Metal-Organic Frameworks for Biomedical Imaging and Drug Delivery. *Acc. Chem. Res.* **2011**, *44* (10), 957–968.

(6) Riccò, R.; Liang, W.; Li, S.; Gassensmith, J. J.; Caruso, F.; Doonan, C.; Falcaro, P. Metal–Organic Frameworks for Cell and Virus Biology: A Perspective. *ACS Nano* **2018**, *12* (1), 13–23.

(7) Falcaro, P.; Ricco, R.; Doherty, C. M.; Liang, K.; Hill, A. J.; Styles, M. J. MOF Positioning Technology and Device Fabrication. *Chem. Soc. Rev.* **2014**, *43* (16), 5513–60.

(8) Scott, A. The next Big Thing, Again. *CEN Glob. Enterp.* **2017**, *95* (24), 18–19.

(9) Frameworks for Commercial Success. *Nat. Chem.* **2016**, *8* (11), 987.

(10) Faust, T. MOFs move to market https://www.nature.com/articles/nchem.2656 (accessed Apr 9, 2018).

(11) Wang, F.; Deng, K.; Wu, G.; Liao, H.; Liao, H.; Zhang, L.; Lan, S.; Zhang, J.; Song, X.; Wen, L. Facile and Large-Scale Syntheses of Nanocrystal Rare Earth Metal–Organic Frameworks at Room Temperature and Their Photoluminescence Properties. *J. Inorg. Organomet. Polym. Mater.* **2012**, *22* (4), 680–685.

(12) Crawford, D.; Casaban, J.; Haydon, R.; Giri, N.; McNally, T.; James, S. L. Synthesis by Extrusion: Continuous, Large-Scale Preparation of MOFs Using Little or No Solvent. *Chem. Sci.* **2015**, *6* (3), 1645–1649.

(13) Bag, P. P.; Wang, X.-S.; Cao, R. Microwave-Assisted Large Scale Synthesis of Lanthanide Metal–organic Frameworks (Ln-MOFs), Having a Preferred Conformation and Photoluminescence Properties. *Dalton Trans.* **2015**, *44* (26), 11954–11962.

(14) Taddei, M.; Steitz, D. A.; van Bokhoven, J. A.; Ranocchiari, M. Continuous-Flow Microwave Synthesis of Metal-Organic Frameworks: A Highly Efficient Method for Large-Scale Production. *Chem. - Eur. J.* **2016**, *22* (10), 3245–3249.

(15) Yang, X.; Guo, X.; Zhang, C.; Yang, Y.; Li, Y. Large Scale Halogen-free Synthesis of Metal-organic Framework Material Fe-MIL-100. *Chin. J. Mater. Res. Cailiao Yanjiu Xuebao* **2017**, *31* (8), 569–575.

(16) Tranchemontagne, D. J.; Hunt, J. R.; Yaghi, O. M. Room Temperature Synthesis of Metal-Organic Frameworks: MOF-5, MOF-74, MOF-177, MOF-199, and IRMOF-0. *Tetrahedron* **2008**, *64* (36), 8553–8557.

(17) de Boer, J.; van Bavel, B. Tools for the REACH Programme - Analytical Methods for the Evaluation of Industrial Contaminants. *J. Chromatogr. A* **2009**, *1216* (3), 301.

(18) Puttlitz, K. J.; Galyon, G. T. Impact of the ROHS Directive on High-Performance Electronic Systems: Part II: Key Reliability Issues Preventing the Implementation of Lead-Free Solders. *J. Mater. Sci. Mater. Electron.* **2006**, *18* (1–3), 347–365.

(19) Sun, Y.; Zhou, H.-C. Recent Progress in the Synthesis of Metal–organic Frameworks. *Sci. Technol. Adv. Mater.* **2015**, *16* (5), 054202.

(20) Bayliss, P. A.; Ibarra, I. A.; Pérez, E.; Yang, S.; Tang, C. C.; Poliakoff, M.; Schröder, M. Synthesis of Metal–organic Frameworks by Continuous Flow. *Green Chem.* **2014**, *16* (8), 3796.

(21) Reinsch, H.; Bueken, B.; Vermoortele, F.; Stassen, I.; Lieb, A.; Lillerud, K.-P.; De Vos, D. Green Synthesis of Zirconium-MOFs. *CrystEngComm* **2015**, *17* (22), 4070–4074.

(22) Reinsch, H.; Waitschat, S.; Chavan, S. M.; Lillerud, K. P.; Stock, N. A Facile "Green" Route for Scalable Batch Production and Continuous Synthesis of Zirconium MOFs: A Facile "Green" Route for Scalable Batch Production and Continuous Synthesis of Zirconium MOFs. *Eur. J. Inorg. Chem.* **2016**, *2016* (27), 4490–4498.

(23) Klimakow, M.; Klobes, P.; Thünemann, A. F.; Rademann, K.; Emmerling, F. Mechanochemical Synthesis of Metal–Organic Frameworks: A Fast and Facile Approach toward Quantitative Yields and High Specific Surface Areas. *Chem. Mater.* **2010**, *22* (18), 5216–5221.

(24) Užarević, K.; Wang, T. C.; Moon, S.-Y.; Fidelli, A. M.; Hupp, J. T.; Farha, O. K.; Friščić, T. Mechanochemical and Solvent-Free Assembly of Zirconium-Based Metal–organic Frameworks. *Chem Commun* **2016**, *52* (10), 2133–2136.

(25) Ricco, R.; Pfeiffer, C.; Sumida, K.; Sumby, C. J.; Falcaro, P.; Furukawa, S.; Champness, N. R.; Doonan, C. J. Emerging Applications of Metal–organic Frameworks. *CrystEngComm* **2016**, *18* (35), 6532–6542.

(26) Reboul, J.; Furukawa, S.; Horike, N.; Tsotsalas, M.; Hirai, K.; Uehara, H.; Kondo, M.; Louvain, N.; Sakata, O.; Kitagawa, S. Mesoscopic Architectures of Porous Coordination Polymers Fabricated by Pseudomorphic Replication. *Nat. Mater.* **2012**, *11* (8), 717–23.

(27) Stassen, I.; Styles, M.; Grenci, G.; Gorp, H. V.; Vanderlinden, W.; Feyter, S. D.; Falcaro, P.; Vos, D. D.; Vereecken, P.; Ameloot, R. Chemical Vapour Deposition of Zeolitic Imidazolate Framework Thin Films. *Nat. Mater.* **2015**, *15* (3), 304–310.

(28) Falcaro, P.; Okada, K.; Hara, T.; Ikigaki, K.; Tokudome, Y.; Thornton, A. W.; Hill, A. J.; Williams, T.; Doonan, C.; Takahashi, M. Centimetre-Scale Micropore Alignment in Oriented Polycrystalline Metal-Organic Framework Films via Heteroepitaxial Growth. *Nat. Mater.* **2017**, *16* (3), 342–348.

(29) Sumida, K.; Hu, M.; Furukawa, S.; Kitagawa, S. Structuralization of $Ca^{2+}$-Based Metal–Organic Frameworks Prepared via Coordination Replication of Calcium Carbonate. *Inorg. Chem.* **2016**, *55* (7), 3700–3705.

(30) Liang, K.; Ricco, R.; Doherty, C. M.; Styles, M. J.; Bell, S.; Kirby, N.; Mudie, S.; Haylock, D.; Hill, A. J.; Doonan, C. J.; et al. Biomimetic Mineralization of Metal-Organic Frameworks as Protective Coatings for Biomacromolecules. *Nat. Commun.* **2015**, *6*, 7240.

(31) Zanchetta, E.; Malfatti, L.; Ricco, R.; Styles, M. J.; Lisi, F.; Coghlan, C. J.; Doonan, C. J.; Hill, A. J.; Brusatin, G.; Falcaro, P. ZnO as an Efficient Nucleating Agent for Rapid, Room Temperature Synthesis and Patterning of Zn-Based Metal–Organic Frameworks. *Chem. Mater.* **2015**, *27* (3), 690–699.

(32) Süsse, P. Verfeinerung Der Kristallstruktur Des Malachits, $Cu_2(OH)_2CO_3$. *Acta Crystallogr.* **1967**, *22* (1), 146–151.

(33) Gattow, G.; Zemann, J. Neubestimmung Des Kristallstruktur von Azurit, $Cu_3(OH)_2(CO_3)_2$. *Acta Crystallogr.* **1958**, *11* (12), 866–872.

(34) Lluveras, A.; Boularand, S.; Andreotti, A.; Vendrell-Saz, M. Degradation of Azurite in Mural Paintings: Distribution of Copper Carbonate, Chlorides and Oxalates by SRFTIR. *Appl. Phys. A* **2010**, *99* (2), 363–375.

(35) Okada, K.; Ricco, R.; Tokudome, Y.; Styles, M. J.; Hill, A. J.; Takahashi, M.; Falcaro, P. Copper Conversion into $Cu(OH)_2$ Nanotubes for Positioning $Cu_3(BTC)_2$ MOF Crystals: Controlling the Growth on Flat Plates, 3D Architectures, and as Patterns. *Adv. Funct. Mater.* **2014**, *24* (14), 1969–1977.

(36) Moitra, N.; Fukumoto, S.; Reboul, J.; Sumida, K.; Zhu, Y.; Nakanishi, K.; Furukawa, S.; Kitagawa, S.; Kanamori, K. Mechanically Stable, Hierarchically Porous $Cu_3(Btc)_2$ (HKUST-1) Monoliths via Direct Conversion of Copper(II) Hydroxide-Based Monoliths. *Chem. Commun. Camb. Engl.* **2015**, *51* (17), 3511–4.

(37) Toyao, T.; Liang, K.; Okada, K.; Ricco, R.; Styles, M. J.; Tokudome, Y.; Horiuchi, Y.; Hill, A. J.; Takahashi, M.; Matsuoka, M.; et al. Positioning of the HKUST-1 Metal–organic Framework ($Cu_3(BTC)_2$) through Conversion from Insoluble Cu-Based Precursors. *Inorg Chem Front* **2015**, *2* (5), 434–441.

(38) Guo, Y.; Mao, Y.; Hu, P.; Ying, Y.; Peng, X. Self–confined Synthesis of HKUST-1 Membranes from CuO Nanosheets at Room Temperature. *ChemistrySelect* **2016**, *1* (1), 108–113.

(39) Millward, A. R.; Yaghi, O. M. Metal–Organic Frameworks with Exceptionally High Capacity for Storage of Carbon Dioxide at Room Temperature. *J. Am. Chem. Soc.* **2005**, *127* (51), 17998–17999.

(40) Pérez-Mayoral, E.; Musilová, Z.; Gil, B.; Marszalek, B.; Položij, M.; Nachtigall, P.; Čejka, J. Synthesis of Quinolines via Friedländer Reaction Catalyzed by CuBTC Metal–organic-Framework. *Dalton Trans.* **2012**, *41* (14), 4036.

(41) Wallwork, K. S.; Kennedy, B. J.; Wang, D. The High Resolution Powder Diffraction Beamline for the Australian Synchrotron. In *AIP Conference Proceedings*; AIP Publishing, 2007; Vol. 879, pp 879–882.

(42) Bergamaschi, A.; Cervellino, A.; Dinapoli, R.; Gozzo, F.; Henrich, B.; Johnson, I.; Kraft, P.; Mozzanica, A.; Schmitt, B.; Shi, X. The MYTHEN Detector for X-Ray Powder Diffraction Experiments at the Swiss Light Source. *J. Synchrotron Radiat.* **2010**, *17* (5), 653–668.

(43) Rietveld, H. M. A Profile Refinement Method for Nuclear and Magnetic Structures. *J. Appl. Crystallogr.* **1969**, *2* (2), 65–71.

(44) Amenitsch, H.; Rappolt, M.; Kriechbaum, M.; Mio, H.; Laggner, P.; Bernstorff, S. First Performance Assessment of the Small-Angle X-Ray Scattering Beamline at ELETTRA. *J. Synchrotron Radiat.* **1998**, *5* (3), 506–508.

(45) Brunauer, S.; Emmett, P. H.; Teller, E. Adsorption of Gases in Multimolecular Layers. *J. Am. Chem. Soc.* **1938**, *60* (2), 309–319.

(46) *Characterization of Porous Solids VII: Proceedings of the 7th International Symposium on the Characterization of Porous Solids (COPS-VII), Aix-En-Provence, France, 26-28 May 2005*, 1st ed.; Llewellyn, P. L., Rodríguez Reinoso, F., Rouquerol, J., Seaton, N., Eds.; Studies in surface science and catalysis; Elsevier: Amsterdam, 2007.

(47) Barrett, E. P.; Joyner, L. G.; Halenda, P. P. The Determination of Pore Volume and Area Distributions in Porous Substances. I. Computations from Nitrogen Isotherms. *J. Am. Chem. Soc.* **1951**, *73* (1), 373–380.

(48) Stock, N.; Biswas, S. Synthesis of Metal-Organic Frameworks (MOFs): Routes to Various MOF Topologies, Morphologies, and Composites. *Chem. Rev.* **2012**, *112* (2), 933–969.

(49) Bauer, S.; Stock, N. Implementation of a Temperature-Gradient Reactor System for High-Throughput Investigation of Phosphonate-Based Inorganic–Organic Hybrid Compounds. *Angew. Chem. Int. Ed.* **2007**, *46* (36), 6857–6860.

(50) Forster, P. M.; Stock, N.; Cheetham, A. K. A High-Throughput Investigation of the Role of PH, Temperature, Concentration, and Time on the Synthesis of Hybrid Inorganic-Organic Materials. *Angew. Chem. Int. Ed.* **2005**, *44* (46), 7608–7611.

(51) Bauer, S.; Serre, C.; Devic, T.; Horcajada, P.; Marrot, J.; Férey, G.; Stock, N. High-Throughput Assisted Rationalization of the Formation of Metal Organic Frameworks in the Iron(III) Aminoterephthalate Solvothermal System. *Inorg. Chem.* **2008**, *47* (17), 7568–7576.

(52) Wang, F.; Guo, H.; Chai, Y.; Li, Y.; Liu, C. The Controlled Regulation of Morphology and Size of HKUST-1 by "Coordination Modulation Method." *Microporous Mesoporous Mater.* **2013**, *173* (Supplement C), 181–188.

(53) Guo, H.; Zhu, Y.; Wang, S.; Su, S.; Zhou, L.; Zhang, H. Combining Coordination Modulation with Acid–Base Adjustment for the Control over Size of Metal–Organic Frameworks. *Chem. Mater.* **2012**, *24* (3), 444–450.

(54) Cui, Y.; Chen, B.; Qian, G. Lanthanide Metal-Organic Frameworks for Luminescent Sensing and Light-Emitting Applications. *Coord. Chem. Rev.* **2014**, *273–274* (Supplement C), 76–86.

(55) Küsgens, P.; Rose, M.; Senkovska, I.; Fröde, H.; Henschel, A.; Siegle, S.; Kaskel, S. Characterization of Metal-Organic Frameworks by Water Adsorption. *Microporous Mesoporous Mater.* **2009**, *120* (3), 325–330.

(56) Burtch, N. C.; Jasuja, H.; Walton, K. S. Water Stability and Adsorption in Metal–Organic Frameworks. *Chem. Rev.* **2014**, *114* (20), 10575–10612.

(57) Prestipino, C.; Regli, L.; Vitillo, J. G.; Bonino, F.; Damin, A.; Lamberti, C.; Zecchina, A.; Solari, P. L.; Kongshaug, K. O.; Bordiga, S. Local Structure of Framework Cu(II) in HKUST-1 Metallorganic Framework: Spectroscopic Characterization upon Activation and Interaction with Adsorbates. *Chem. Mater.* **2006**, *18* (5), 1337–1346.

(58) Chui, S. S.-Y.; Lo, S. M.-F.; Charmant, J. P. H.; Orpen, A. G.; Williams, I. D. A Chemically Functionalizable Nanoporous Material [Cu3(TMA)2(H2O)3]N. *Science* **1999**, *283* (5405), 1148–1150.

(59) Bowman, R.; Friedman, A. M.; Lerner, J.; Milsted, J. A Statistical Study of the Impurity Occurrences in Copper Ores and Their Relationship to Ore Types. *Archaeometry* **1975**, *17* (2), 157–163.

(60) Stolar, T.; Batzdorf, L.; Lukin, S.; Žilić, D.; Motillo, C.; Friščić, T.; Emmerling, F.; Halasz, I.; Užarević, K. In Situ Monitoring of the Mechanosynthesis of the Archetypal Metal–Organic Framework HKUST-1: Effect of Liquid Additives on the Milling Reactivity. *Inorg. Chem.* **2017**, *56* (11), 6599–6608.

(61) Loera-Serna, S.; Núñez, L. L.; Flores, J.; López-Simeon, R.; Beltrán, H. I. An Alkaline One-Pot Metathesis Reaction to Give a

[$Cu_3(BTC)_2$] MOF at r.t., with Free Cu Coordination Sites and Enhanced Hydrogen Uptake Properties. *RSC Adv.* **2013**, *3* (27), 10962–10972.

(62) Pérez-Mayoral, E.; Čejka, J. [$Cu_3(BTC)_2$]: A Metal-Organic Framework Catalyst for the Friedländer Reaction. *ChemCatChem* **2011**, *3* (1), 157–159.

(63) Toyao, T.; Styles, M. J.; Yago, T.; Sadiq, M. M.; Riccò, R.; Suzuki, K.; Horiuchi, Y.; Takahashi, M.; Matsuoka, M.; Falcaro, P. $Fe_3O_4$@HKUST-1 and Pd/$Fe_3O_4$@HKUST-1 as Magnetically Recyclable Catalysts Prepared via Conversion from a Cu-Based Ceramic. *CrystEngComm* **2017**, *19* (29), 4201–4210.

(64) Marco-Contelles, J.; Pérez-Mayoral, E.; Samadi, A.; Carreiras, M. do C.; Soriano, E. Recent Advances in the Friedländer Reaction. *Chem. Rev.* **2009**, *109* (6), 2652–2671.

(65) Sachse, A.; Ameloot, R.; Coq, B.; Fajula, F.; Coasne, B.; De Vos, D.; Galarneau, A. In Situ Synthesis of Cu–BTC (HKUST-1) in Macro-/Mesoporous Silica Monoliths for Continuous Flow Catalysis. *Chem. Commun.* **2012**, *48* (39), 4749.

(66) Burtoloso, A. C. B. Copper(II) Acetylacetonate: An Inexpensive Multifunctional Catalyst. *Synlett* **2005**, *2005* (18), 2859–2860.

**Table of Contents**

Basic copper carbonate, also widely available as minerals malachite and azurite, can be easily converted into $Cu_3(BTC)_2$ (HKUST-1) by simple reaction with a hydro-alcoholic solution of trimesic acid, providing a simple, efficient, green, and fast method to obtain Metal Organic Frameworks from natural sources.

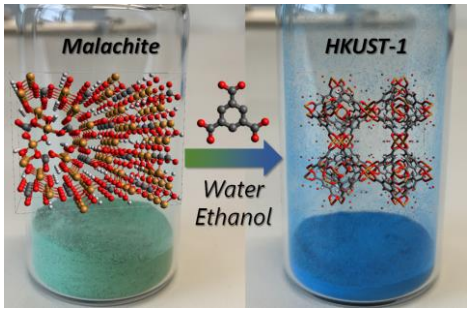

# Supplementary Information

## Direct conversion of Copper Carbonate substrates into porous Metal-Organic Framework HKUST-1.

Raffaele Riccò,[a] Oliver M. Linder-Patton,[b] Kenji Sumida,[b] Mark J. Styles,[c] Kang Liang,[c†] Heinz Amenitsch,[d] Christian J. Doonan,[b] and Paolo Falcaro[a*]

a. Institute of Physical and Theoretical Chemistry, Technical University Graz, Stremayrgasse 9, 8010 Graz, Austria.
b. Department of Chemistry, School of Physical Sciences, The University of Adelaide, North Terrace Campus, Adelaide SA 5005, Australia.
c. CSIRO Manufacturing Flagship, Private Bag 10, 3169 Clayton South MDC, Victoria, Australia.
d. Institute of Inorganic Chemistry, Graz University of Technology, Stremayrgasse 9, 8010 Graz, Austria.

**CONTENTS:**

**Table S1.** BET data related to Figures 2a, S4, and S5

| Fig. | Substrate | Solvent | Temperature | Time | Surface Area ± Error ($m^2/g$) | Note |
|---|---|---|---|---|---|---|
| 2a | BCC, 20 mg | EtOH/water 1:1 | 24 °C | 3 h | 2089 ± 2 | |
| 2a/S5 | BCC, 200 mg | " | " | " | 1569 ± 1 | * |
| 2a | BCC, 2000 mg | " | " | " | 477.6 ± 0.5 | |
| 2b | BCC, 200 mg | " | -78 °C | " | 1076 ± 0.1 | |
| 2b | " | " | 24 °C | " | 1569 ± 1 | * |
| 2b | " | " | 80 °C | " | 1230 ± 0.6 | |
| 2c/S4a | " | EtOH | 24 °C | 20 min | 25.32 ± 0.05 | |
| 2c/S4a | " | " | " | 3 h | 47.4 ± 0.1 | |
| 2c/S4a | " | " | " | 24 h | 160.9 ± 0.3 | |
| 2c/S4b | " | EtOH/water 1:1 | " | 20 min | 1364.9 ± 0.6 | |
| 2c/S4b | " | " | " | 3 h | 1569 ± 1 | * |
| 2c/S4b | " | " | " | 24 h | 901.1 ± 0.2 | |
| 2c/S4c | " | Water | " | 20 min | 128.73 ± 0.08 | |
| 2c/S4c | " | " | " | 3 h | 86.72 ± 0.03 | |
| 2c/S4c | " | " | " | 24 h | 7.65 ± 0.03 | |
| S5 | Malachite | EtOH/water 1:1 | " | 3 h | 742.2 ± 0.3 | |
| S5 | Azurite | " | " | " | 341.4 ± 0.4 | |
| S5 | Solvothermal | " | " | " | 1016 ± 2 | |
| S6 | BCC, 200 mg | " | " | " | 1263.6 ± 0.3 | |
| S6 | " | " | " | " | 63.33 ± 0.07 | ** |

*: same sample
**: previous sample after 24 hours of water treatment

**Figure S1.** Photographs of BCC conversion into HKUST-1 at different amount of starting material.

**Figure S2.** SEM images of HKUST-1 MOFs from basic copper carbonate (BCC) at different amounts of basic copper carbonate.

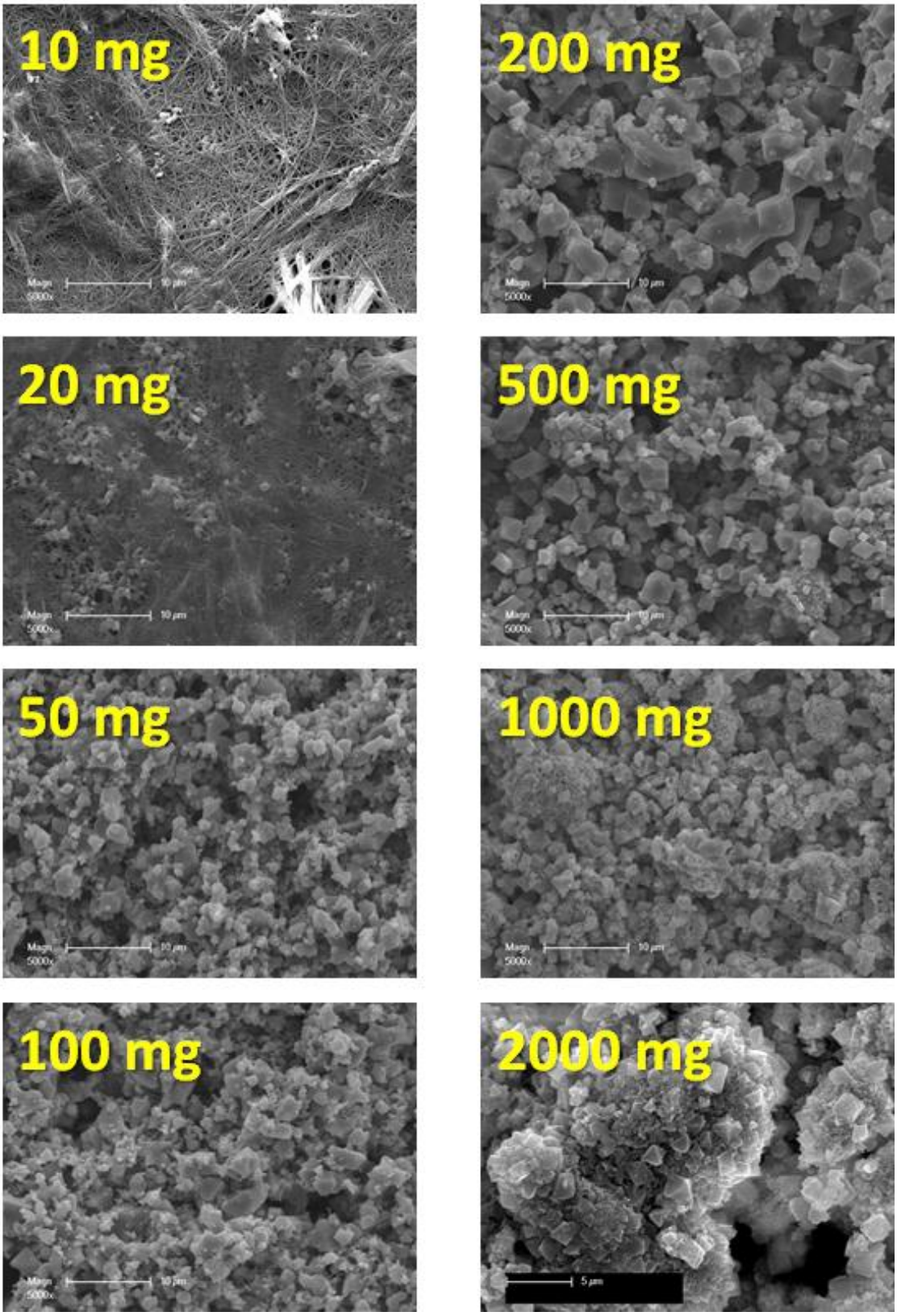

**Figure S3.** SEM images of HKUST-1 MOFs from BCC at different temperatures.

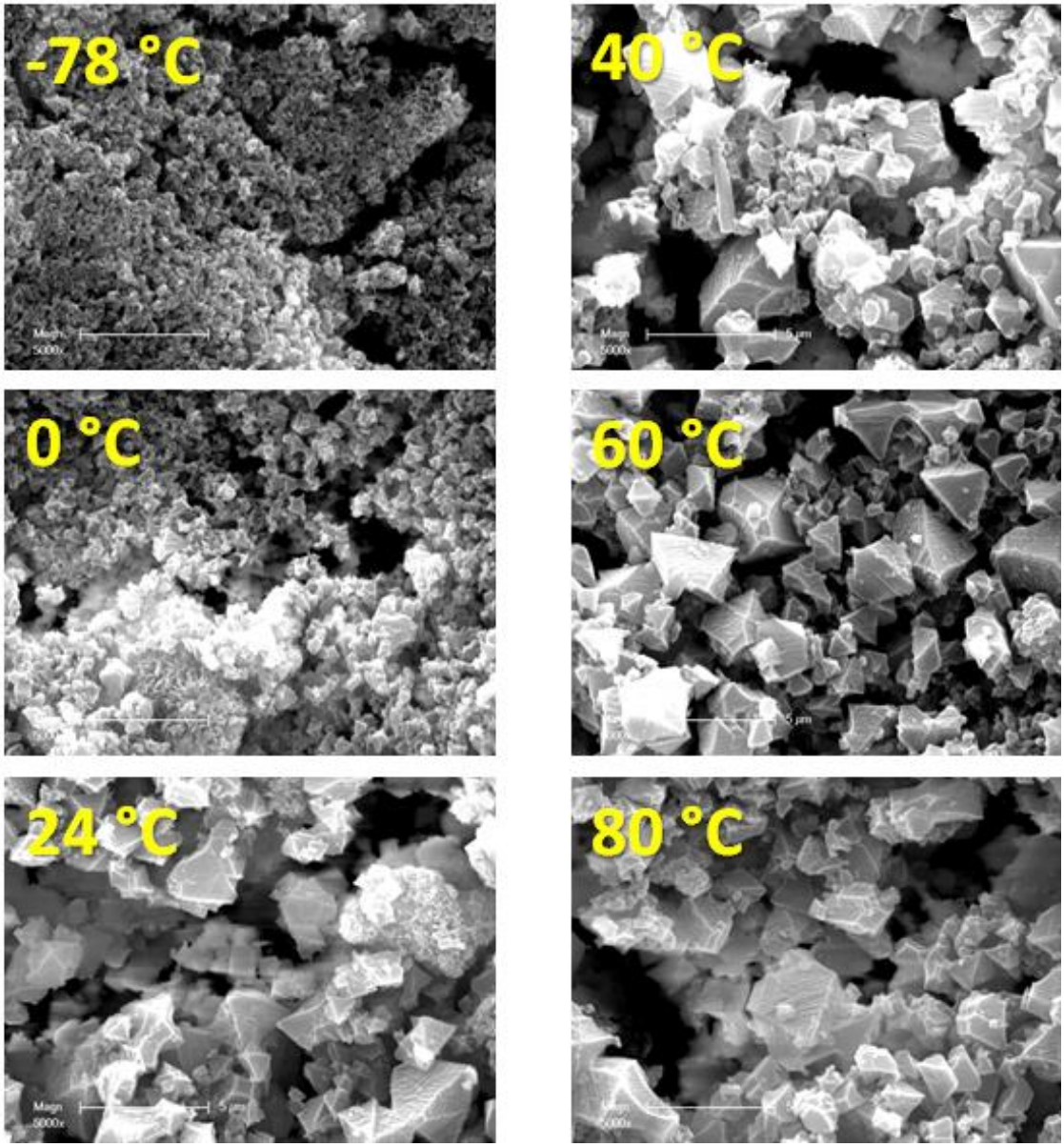

**Figure S4.** SEM images of HKUST-1 MOFs from BCC at different solvent mixtures and times.

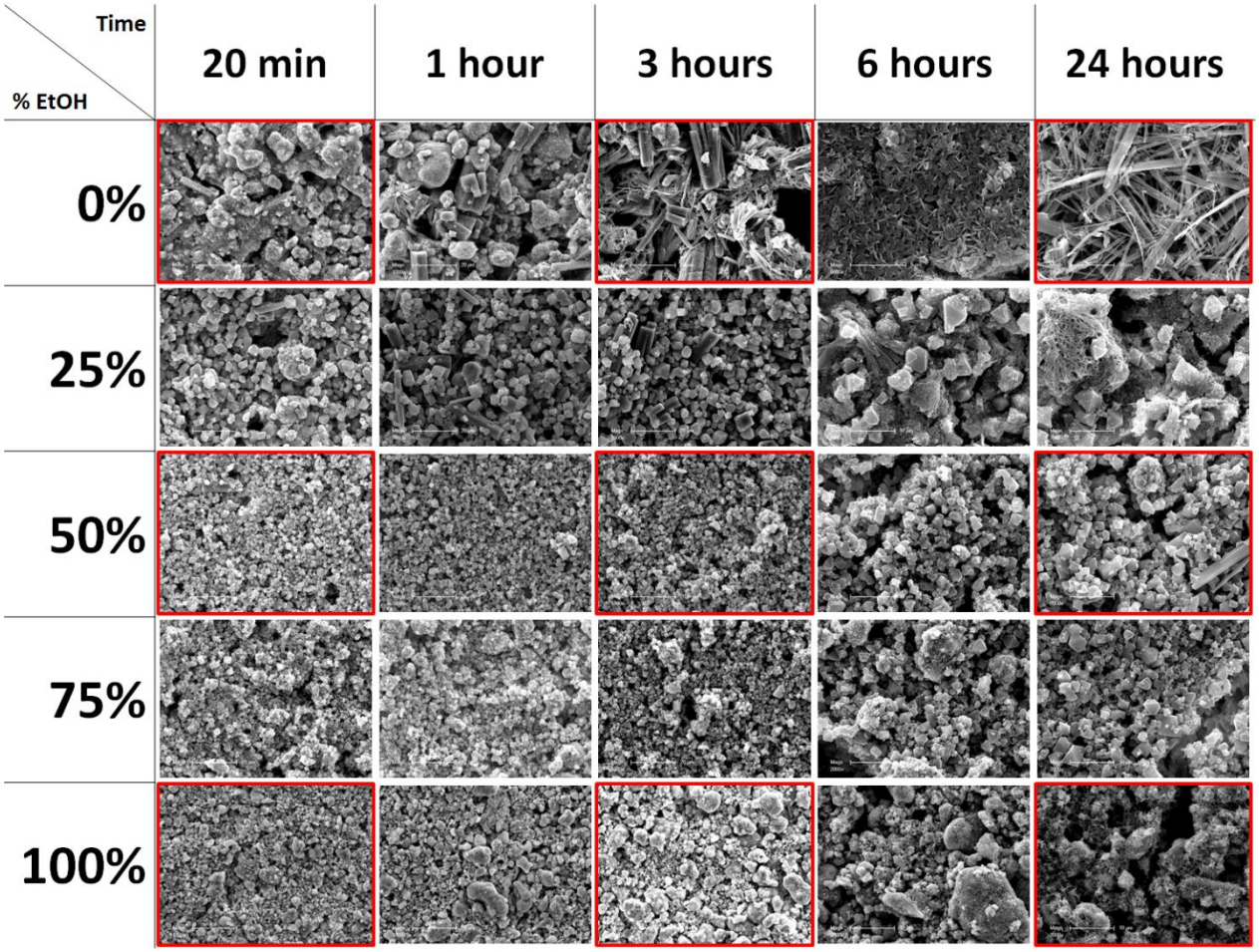


Note: the pictures bordered in red are reported in the main text as Figure 1g-r

**Figure S5.** BET graphs of HKUST-1 MOF from BCC at different solvent mixtures and times.

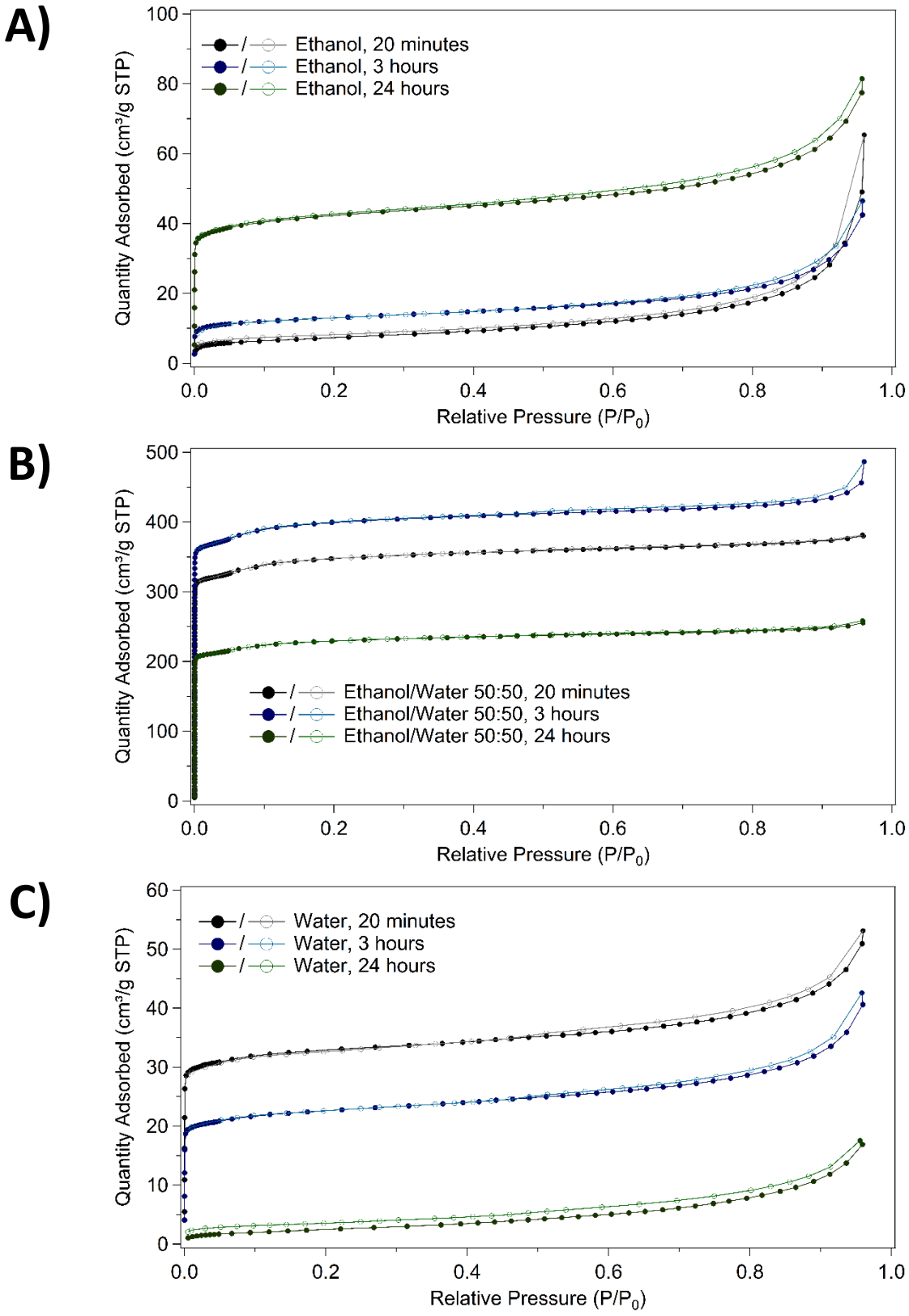

**Figure S6.** A) BET graphs and B) XRD analysis of HKUST-1 MOF from BCC before and after 24 hours of washing in water.

**A)**

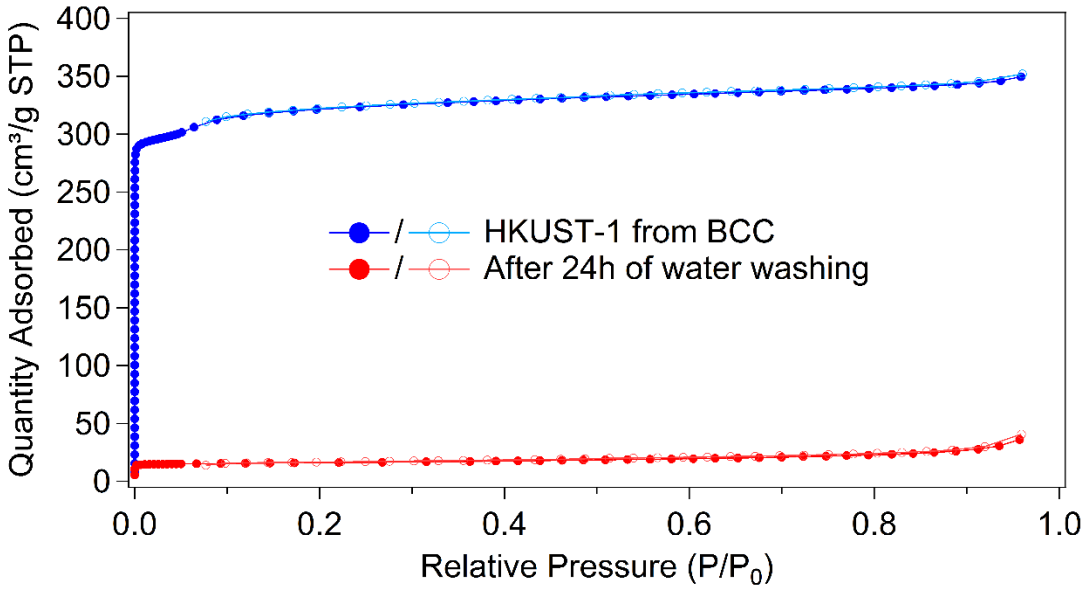


**B)**

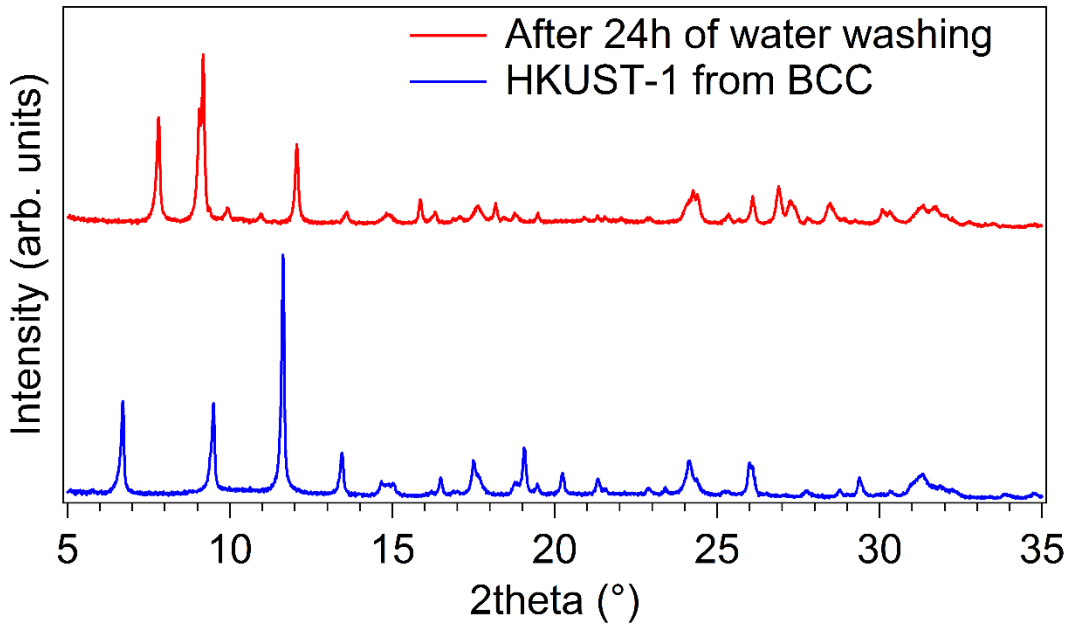

**Figure S7.** Photographs of azurite and malachite minerals before and after HKUST-1 conversion.

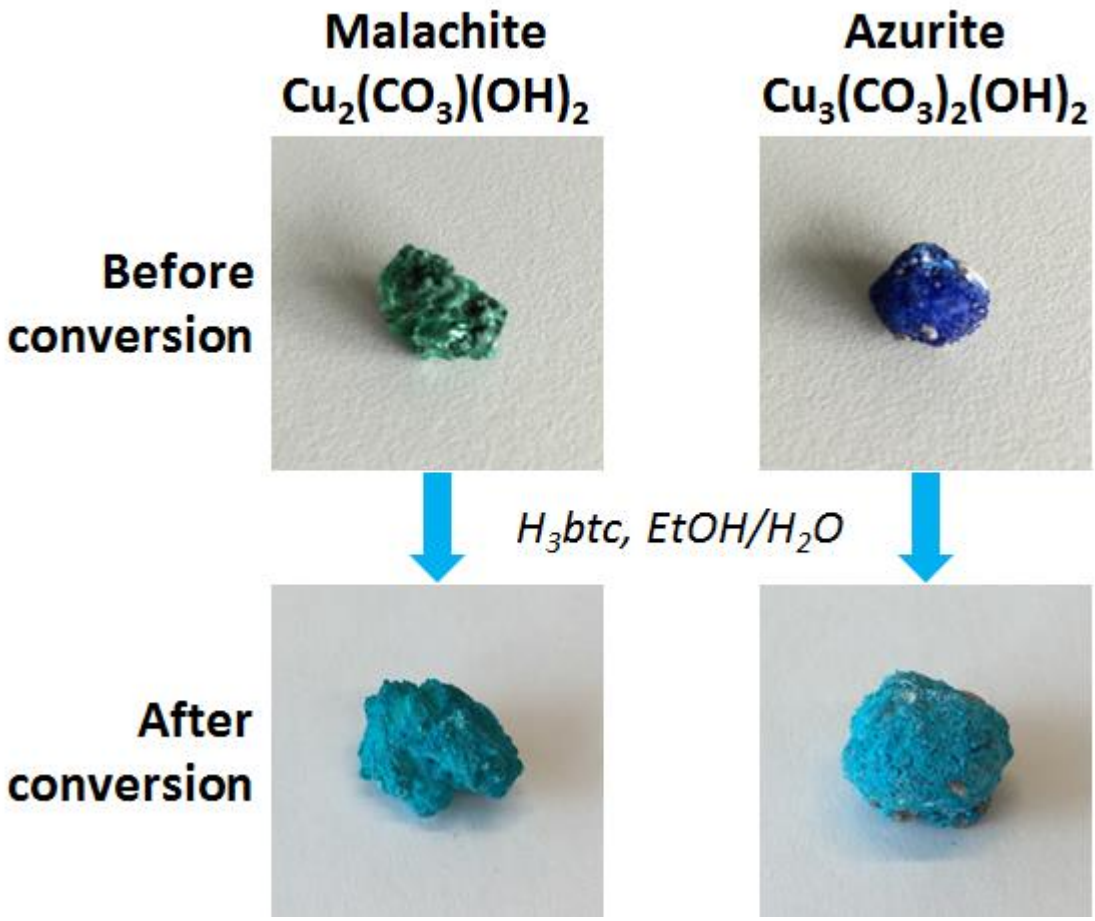

**Figure S8.** BET graphs of HKUST-1 MOF from BCC, malachite, azurite, and solvothermal reaction.

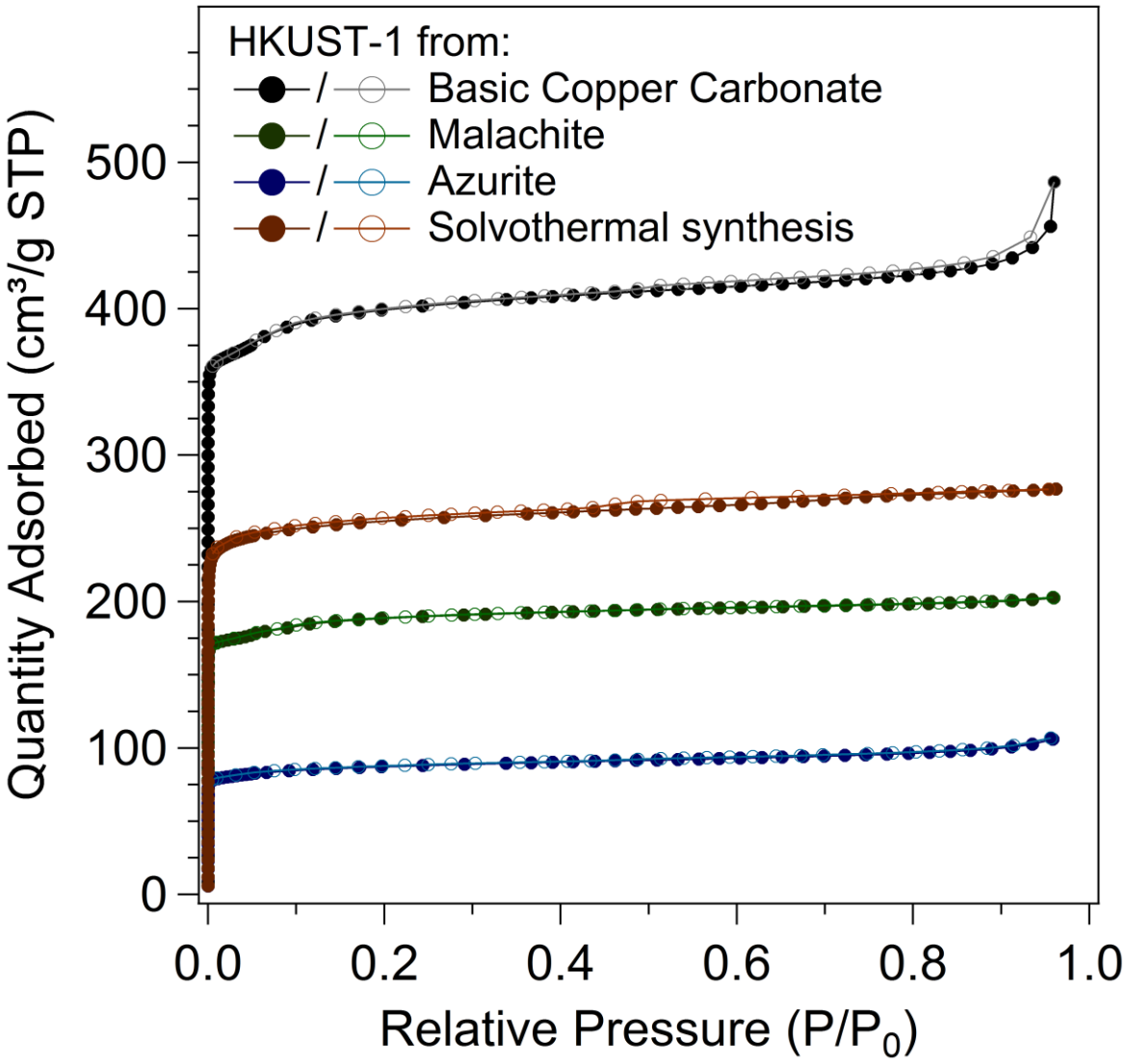

**Figure S9.** Setups used for XRD and SAXS/WAXS experiments

XRD experimental setup with a capillary in static conditions, as performed at the Powder Diffraction Beamline of the Australian Synchrotron, located in Melbourne. For these measurements, the Cu-based precursor material (BCC with particles having diameters of tens of micrometres) was filled into the capillary and the trimesic acid solution in EtOH and water was injected thereafter with a syringe. Due to the logistic setup and the operational requirements of the beamline, it was not possible to collected the initial 2 minutes of reaction, and this is reflected in the XRD kinetics in Figure S12, which starts directly showing the intermediate.

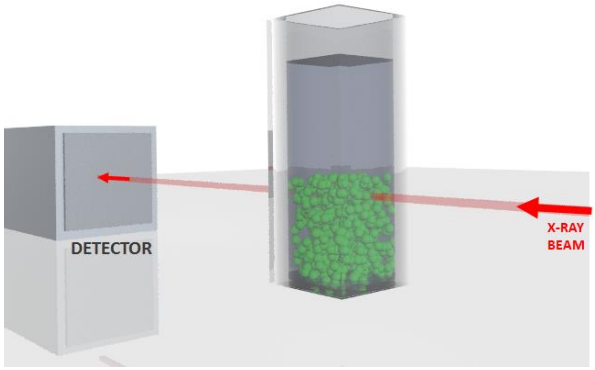


SAXS/WAXS experimental setup using a recirculator in dynamic conditions, as performed at the AustroSAXS Beamline of the Elettra Synchrotron, located in Trieste (Italy). For these measurements, the Cu-based precursor material (BCC with particles having diameters of tens of micrometres) was suspended in EtOH and water, and recirculated through a capillary, connected with a peristaltic pump and a reactor. The trimesic acid solution in EtOH and water was injected at the desired time in the reactor with a remotely controlled syringe pump. With this setup, it was possible to observe the first moments of reaction and obtaining information about the quick disappearance of the carbonate, followed by the formation of a transient intermediate, to the final HKUST-1 conversion.

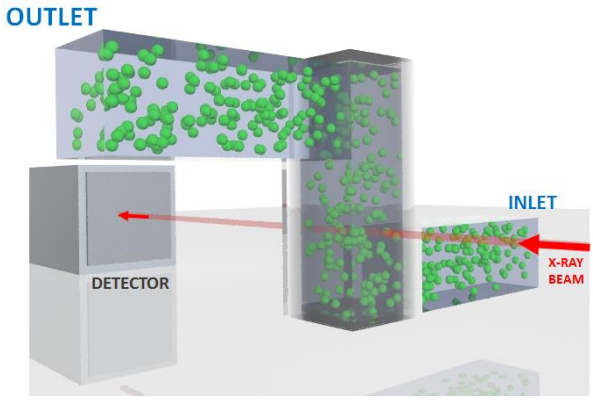

**Figure S10.** Full WAXS kinetics (above) and selected frames at different times (below; initial, after 8, 25, 28, and 60 minutes of reaction). The WAXS shows two additional and weak peaks for the intermediate at q = 7.1 and 7.6 $nm^{-1}$ (2θ = 10.0 and 10.7°), previously unreported by Stolar et al. (ref. 60 of the main text).

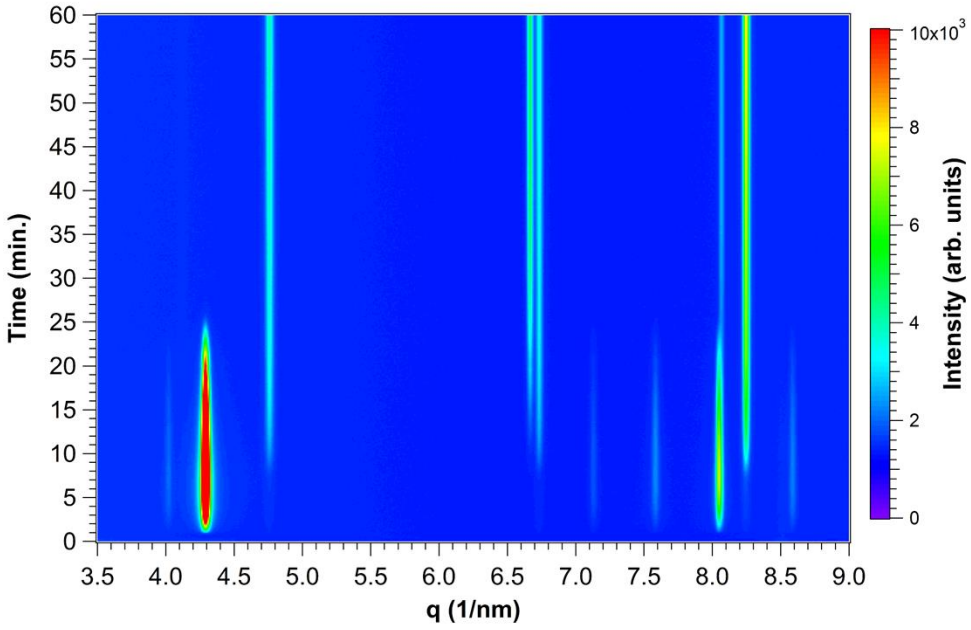


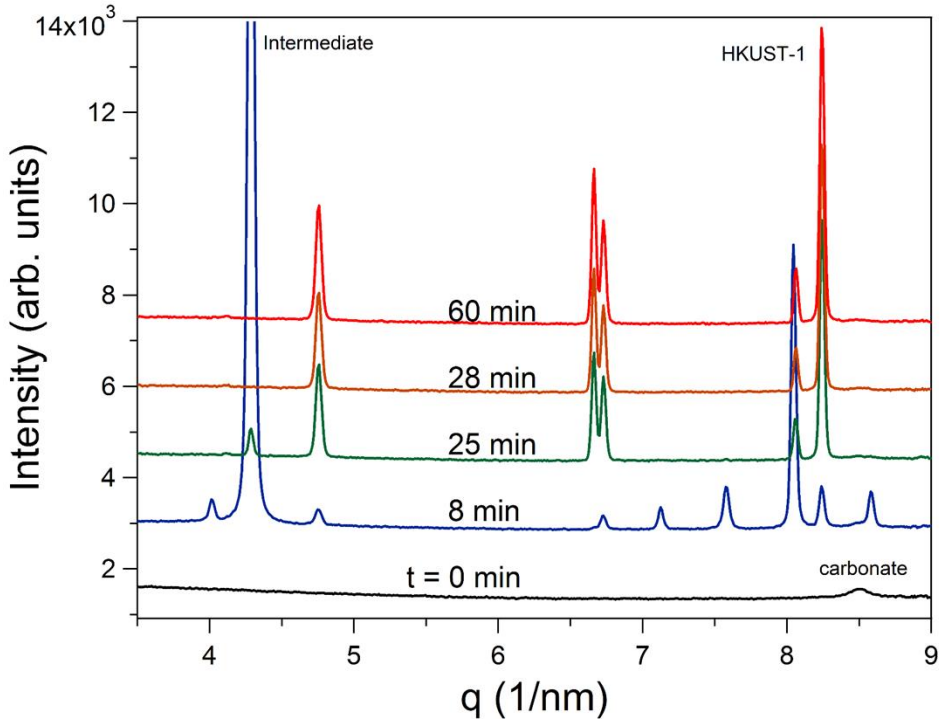

**Figure S11.** Time evolution of the integrated peaks of the intermediate structure (red), HKUST-1 (black) and the copper carbonate precursor (blue) at q =8.5 $nm^{-1}$. Immediately after the addition of $H_3btc$, the Cu-based precursor material (BCC with particles having diameters of tens of micrometres) converts into a growing intermediate structure and partially into HKUST-1, which starts to from faster by the conversion of the intermediate. Remark: the increase of the intensity of carbonate is related to the formation of the intermediate structure occurring at the same peak position.

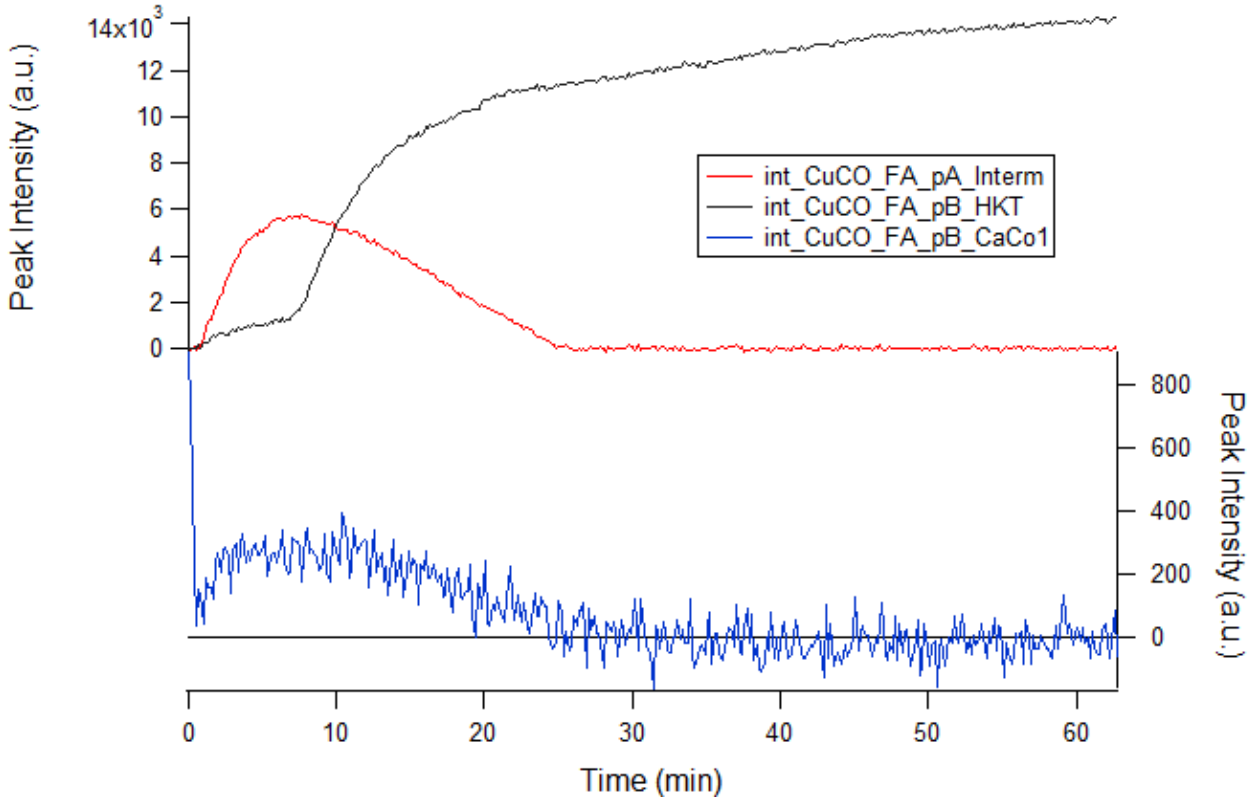

**Figure S12.** a) XRD kinetics analysis conducted at the Powder Diffraction Beamline of the Australian Synchrotron. Remark: the starting time reflects the first acquired frame, however the first 2 minutes of kinetics were not collected; b) Rietveld refinements of final XRD spectra kinetics at 30 minutes.

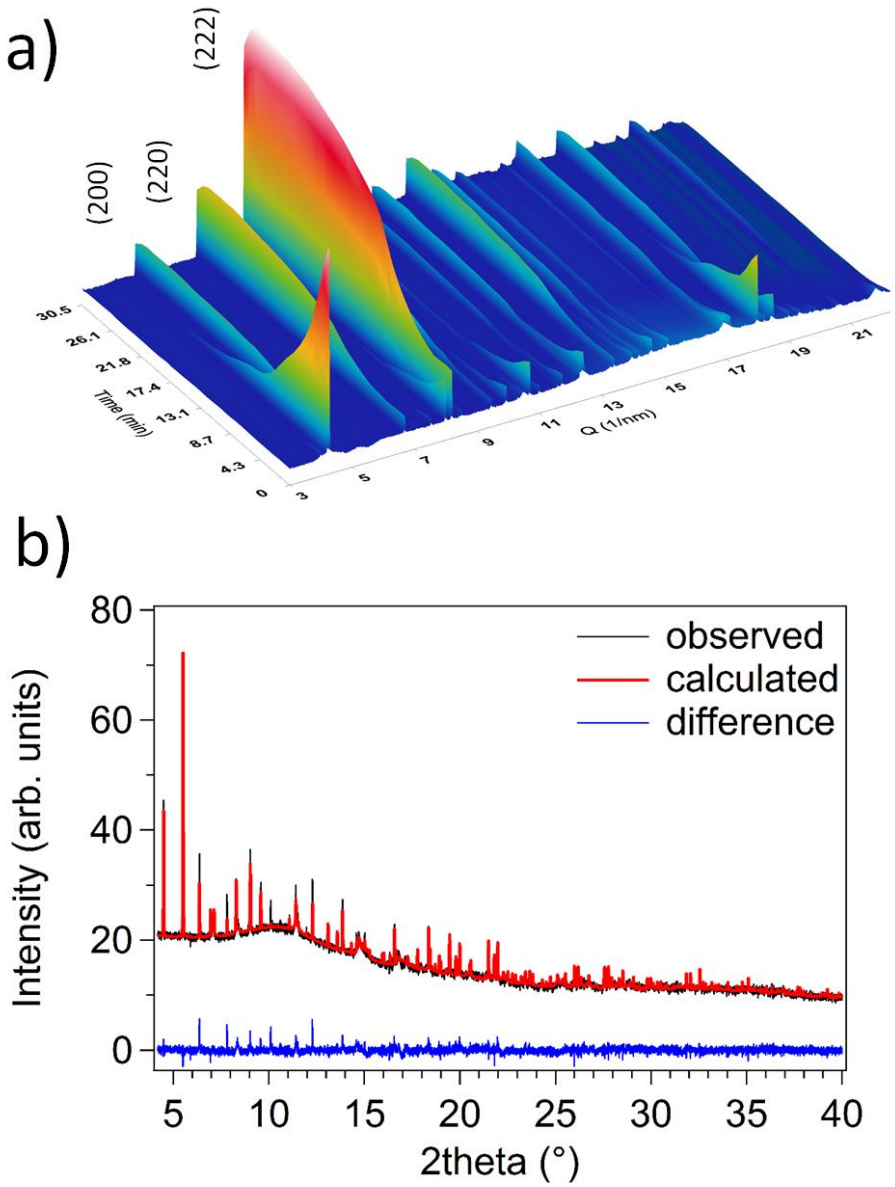

**Figure S13.** FTIR kinetics data of the carbonate-to-HKUST-1 conversion (200 mg carbonate, 6.5 mL of trimesic acid solution) in the first 24 minutes of reaction. Residual peaks attributed to the not yet converted carbonate (●) can be observed along with the peaks of the already obtained HKUST-1 MOF (explicated wavenumbers). The residual peak at 1705 $cm^{-1}$ appears to be consistent with the presence of intermediate at this time of reaction, as similarly reported by Stolar et al. (see ref. 60 of the main text).

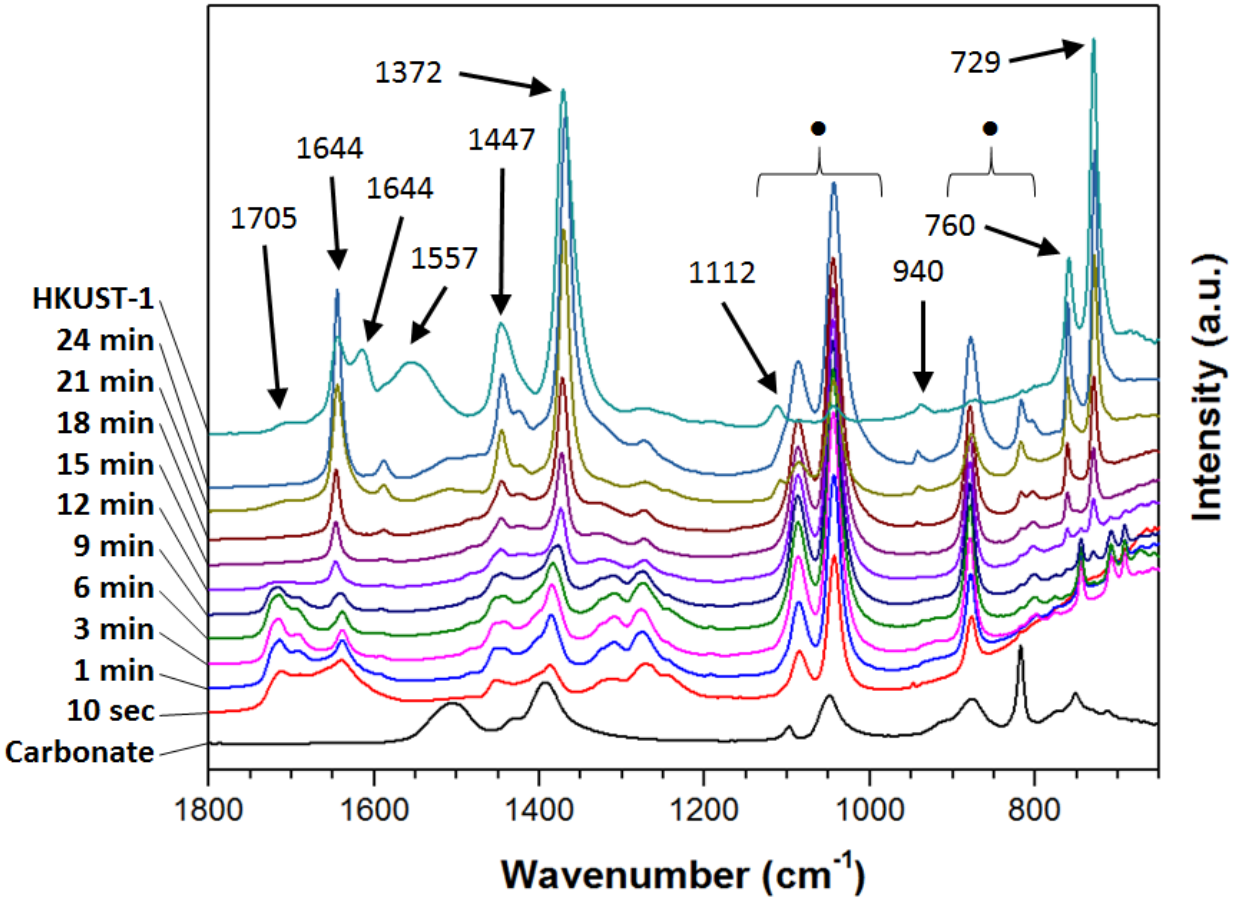

**Figure S14.** [1]H-NMR spectra of the Friedländer reaction performed: using HKUST-1 MOF from BCC, malachite, azurite, and solvothermal reaction; with the related carbonate sources; without catalyst, using copper sulphate, and $H_3BTC$ ligand.

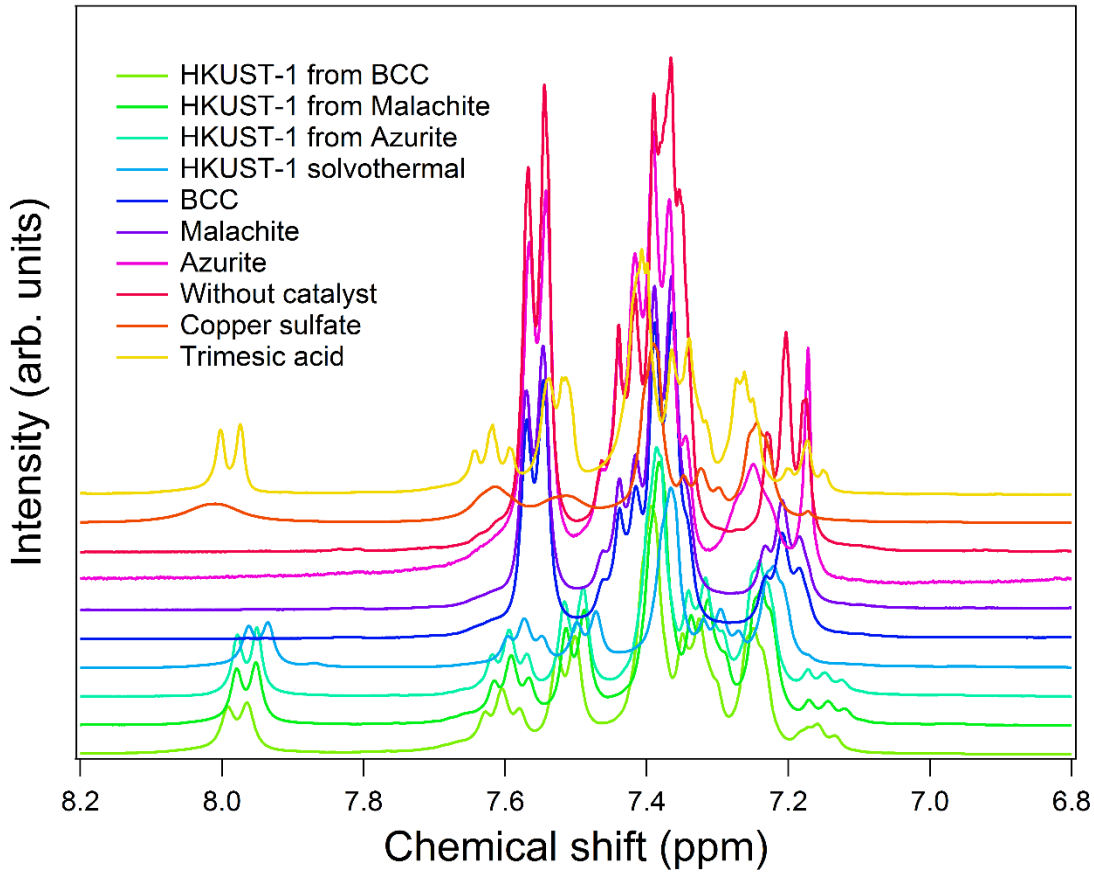

**Figure S15.** $^{1}$H-NMR spectra of the Cu leaching test and relative yields.

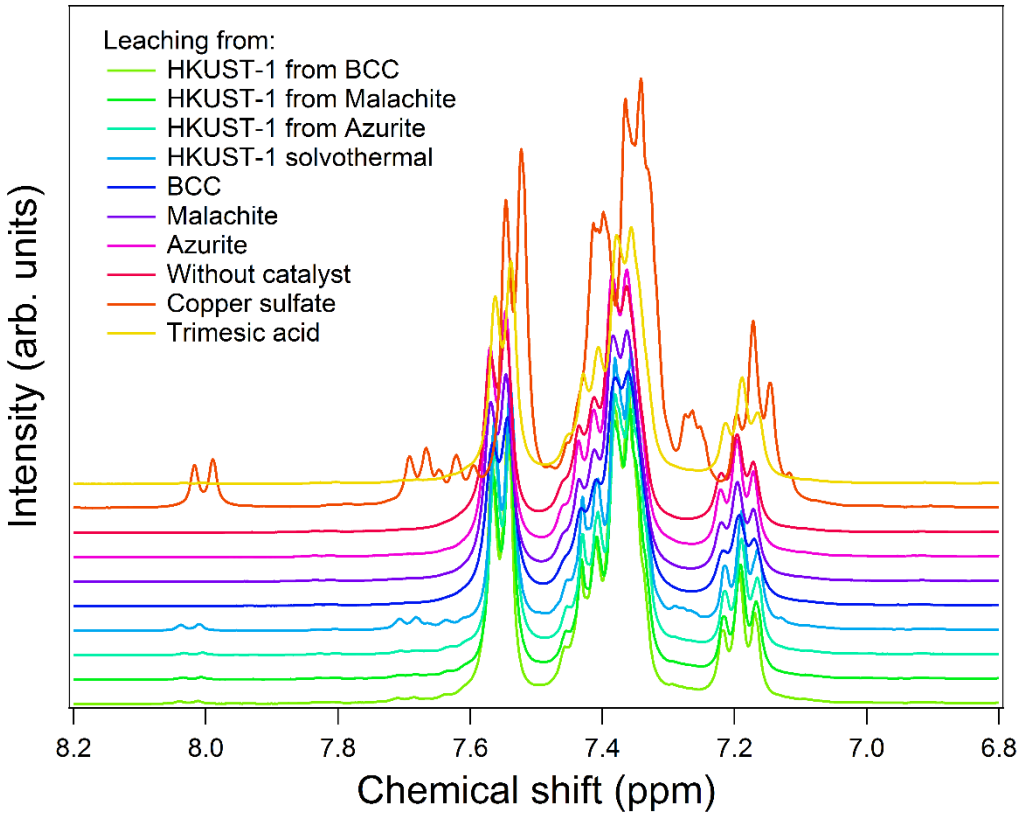

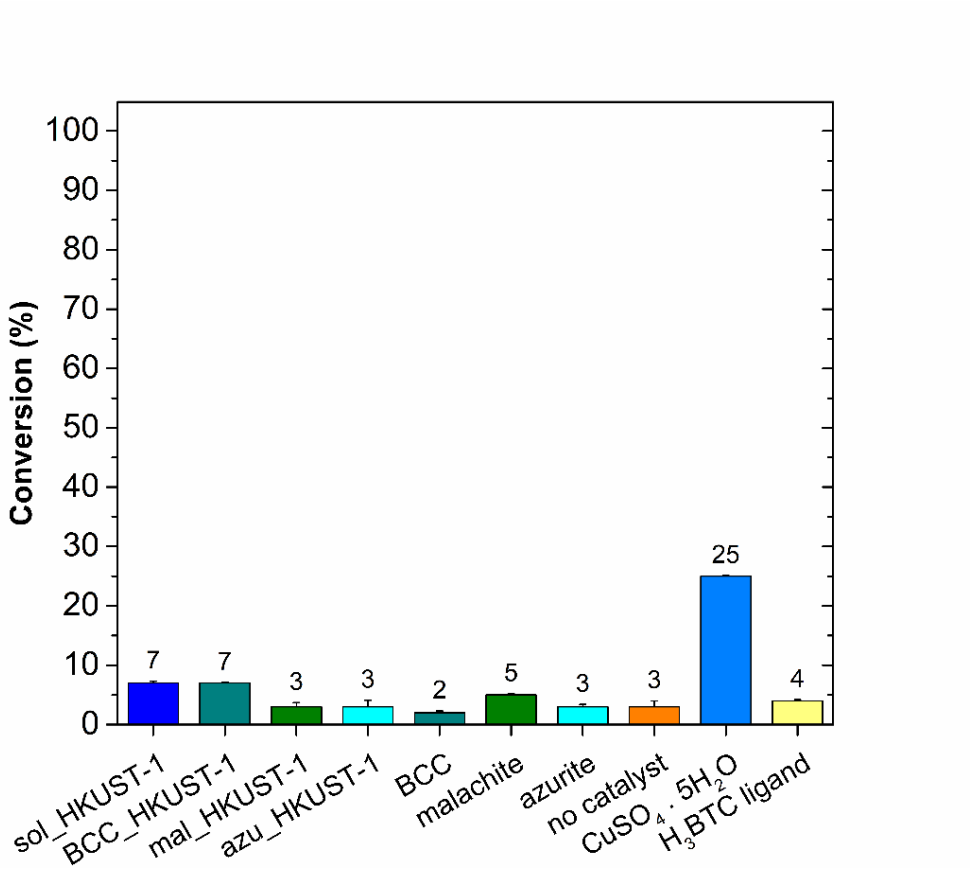
Conversion (%)
100
90
80
70
60
50
40
30
20
10
0
7
7
3
3
2
5
3
3
25
4
sol_HKUST-1
BCC_HKUST-1
mal_HKUST-1
azu_HKUST-1
BCC
malachite
azurite
no catalyst
CuSO4 · 5H2O
H3BTC ligand